Description and evaluation of the Community Multiscale Air Quality (CMAQ) modeling system version 5.1

K. Wyat Appel[1], Sergey L. Napelenok[1], Kristen M. Foley[1], Havala O. T. Pye[1], Christian Hogrefe[1], Deborah J. Luecken[1], Jesse O. Bash[1], Shawn J. Roselle[1], Jonathan E. Pleim[1], Hosein Foroutan[1], William T. Hutzell[1], George A. Pouliot[1], Golam Sarwar[1], Kathleen M. Fahey[1], Brett Gantt[3], Robert C. Gilliam[1], Nicholas K. Heath[1], Daiwen Kang[1], Rohit Mathur[1], Donna B. Schwede[1], Tanya L. Spero[2], David C. Wong[1], Jeffrey O. Young[1]

[1]Computational Exposure Division, National Exposure Research Laboratory, Office of Research and Development, U.S. Environmental Protection Agency, RTP, NC
[2]Systems Exposure Division, National Exposure Research Laboratory, Office of Research and Development, U.S. Environmental Protection Agency, RTP, NC
[3]Air Quality Analysis Division, Office of Air Quality Planning and Standards, Office of Air and Radiation, U.S. Environmental Protection Agency, RTP, NC

Correspondence to: K.Wyat Appel (appel.wyat@epa.gov)

Abstract. The Community Multiscale Air Quality (CMAQ) model is a comprehensive multi-pollutant air quality modeling system developed and maintained by the U.S. Environmental Protection Agency's (EPA) Office of Research and Development (ORD). Recently version 5.1 of the CMAQ model (v5.1) was released to the public, incorporating a large number of science updates and extended capabilities over the previous release version of the model (v5.0.2). These updates include improvements in the meteorological calculations in both CMAQ and the Weather Research and Forecast (WRF) model used to provide meteorological fields to CMAQ; updates to the gas and aerosol chemistry; revisions to the calculations of clouds and photolysis; and improvements to the dry and wet deposition in the model. Sensitivity simulations isolating several of the major updates to the modeling system show that changes to the meteorological calculations result in enhanced afternoon and early evening mixing in the model, periods when the model historically underestimates mixing. This enhanced mixing results is higher ozone (O_3) mixing ratios on average due to reduced NO titration, and lower fine particulate matter ($PM_{2.5}$) concentrations due to greater dilution of primary pollutants (e.g. elemental and organic carbon). Updates to the clouds and photolysis calculations greatly improve consistency between the WRF and CMAQ models and result in generally higher O_3 mixing ratios, primarily due to reduced cloudiness and attenuation of photolysis in the model. Updates to the aerosol chemistry result in higher secondary organic aerosol (SOA) concentrations in the summer, thereby reducing summertime $PM_{2.5}$ bias ($PM_{2.5}$ is typically underestimated by CMAQ in the summer), while updates to the gas chemistry results in slightly higher O_3 and $PM_{2.5}$ on average in January and July. Overall, the seasonal variation in simulated $PM_{2.5}$ generally improves in CMAQv5.1 (when considering all model updates), as $PM_{2.5}$ concentrations decrease in the winter (when $PM_{2.5}$ is generally overestimated) and increase in the summer (when $PM_{2.5}$ is generally underestimated). Ozone mixing ratios are higher on average with v5.1 versus v5.0.2, resulting in higher O_3 mean bias, as O_3 tends to be overestimated by CMAQ throughout most of the year (especially at locations where the observed O_3 is low), however O_3 correlation is largely improved with v5.1. Sensitivity simulations for several hypothetical emission reduction scenarios show that v5.1 tends to be slightly more responsive to reductions in NO_X ($NO + NO_2$), VOC and SO_X ($SO_2 + SO_4$) emissions than v5.0.2, representing an improvement as previous studies have shown CMAQ to underestimate the observed reduction in O_3 due to large, widespread reductions in observed emissions.

Keywords

1 Introduction

Numerous Federal (e.g. United States Environmental Protection Agency (USEPA)), State and private entities rely on numerical model simulations of atmospheric chemistry, transport and deposition of airborne emissions and the resulting pollutants as part of their decision-making process for air quality management and mitigation (e.g. Scheffe et al., 2007). Chemical Transport Models (CTMs), such as the Community Multiscale Air Quality (CMAQ) model (Byun and Schere, 2006), are often employed to provide information about the potential effects of emission control strategies (e.g. Fann et al., 2009), climate change (e.g. Nolte et al., 2008), and provide next-day air quality forecasts (e.g. Eder et al., 2006) in order to inform and protect the public from potentially harmful air pollutants. Since these models are often used to inform the standard setting and implementation for criteria pollutants (e.g. ozone (O_3) and fine particulate matter ($PM_{2.5}$)), they must be maintained at the state-of-the-science. New versions of the CMAQ model have been released periodically over the past fifteen years, with each new version consisting of numerous updates to the scientific algorithms within the model, while also improving the quality of the input data used. Collectively, these updates are aimed at improving the underlying science of atmospheric dynamics and chemistry represented in the model, extending the capabilities for emerging applications, and reducing systematic biases in the modeling system. Every new release of the CMAQ model undergoes extensive evaluation in order to establish its credibility (e.g. Mebust et al., 2003; Appel et al., 2007, 2008, 2013; Foley et al., 2010) and documents its performance relative to previous versions. Most recently, the CMAQ modeling system version 5.1 (v5.1) has been tested and evaluated against observations and was publically released in December 2015 (http://www.cmaq-model.org/).

The scientific upgrades in the CMAQv5.1 modeling system include major revisions to the Pleim-Xiu land-surface model (PX-LSM; Pleim and Xiu, 1995) and the Asymmetric Convective Mixing version 2 (ACM2; Pleim, 2007ab) planetary boundary layer (PBL) model in the Weather Research and Forecast (WRF) model version 3.7 (Skamarock et al., 2008), which required revisions to the ACM2 scheme in CMAQ to maintain consistency. Corrections were also made to the Monin-Obukhov length (MOL) calculation in CMAQv5.1 to make it consistent with the calculation in the WRF model. The changes to the PX-LSM, ACM2 and MOL calculations in CMAQ had significant impact on the mixing within both WRF and CMAQ, and hence large impacts on the pollutant concentrations in CMAQ. These updates are described in Section 2.1. A new explicit treatment of secondary organic aerosol (SOA) formation from isoprene, alkenes and PAHs was also added in CMAQv5.1. Additionally, two aerosol mechanisms are now available in v5.1, AERO6 and AERO6i (with isoprene extensions), which include updates to the SOA and ISORROPIA algorithms (Nenes et al., 1998; Nenes et al., 1999). The AERO5 mechanism has been deprecated and is no longer available. The updates to the aerosol treatment in v5.1 are described in Section 2.2. Significant changes were also made to the in-line calculation of photolysis rates (described in Section 2.3). Finally, the photochemistry in v5.1 underwent major changes, specifically the photochemical cross sections and quantum yields for the Carbon Bond 2005 e51 (CB05e51) chemical mechanism were updated, along with updates to inorganic and organic chemical reaction rates and products to ensure consistency with the International Union of Pure and Applied Chemistry (IUPAC). And finally the additional representation of organic nitrate species in CB05e51. These updates are described in Section 2.4.

Section 2 provides a brief description of the major scientific and structural improvements included in v5.1. The model configuration and observational data sets used in the model evaluation are provided in Section 3. The evaluation of v5.1 is then presented in two

parts. Section 4 documents the evaluation of several specific changes that were isolated as part of the overall testing of the model. Specifically, Section 4.1 evaluates the meteorological updates in WRF and CMAQ; Section 4.2 evaluates the aerosol updates; Section 4.3 evaluates the changes to the inline photolysis calculation and the representation of clouds within CMAQv5.1; and Section 4.4 evaluates the updates to the CB05e51 chemical mechanism. These increments were chosen as the focus of this paper because they represent a fundamental change from the previously released model version and had the propensity to impact model performance for criteria pollutants. The second portion of the evaluation, presented in Section 5, summarizes the overall change in $PM_{2.5}$ and O_3 model performance with v5.1 compared to the previously released version (CMAQ version 5.0.2 (v5.0.2)). Section 6 provides a discussion of the model response of O_3 and $PM_{2.5}$ to hypothetical reductions in emissions. And finally a summary discussion in provided in Section 7.

2 Review of scientific improvements in CMAQ v5.1

Improvements to the v5.1 modeling system are the result of many years of scientific advancements derived from laboratory, field and numerical experiments and the efforts of a relatively small group of model developers that both investigate avenues for model improvements and then update the model (i.e. write code). Given the large community of CMAQ model users, there are never sufficient resources to diagnose and address every issue in the modeling system that has been reported. As such, it is necessary to prioritize updates to the model based on many different factors, including results from evaluations of past model versions, existing and upcoming regulatory needs, emerging scientific issues, requests from the CMAQ user community, and the expertise within the model developer group to meet those needs/requests. The updates presented herein represent the "major" updates made to the CMAQ modeling system from the previous model version, and therefore does not constitute a fully comprehensive description of all the changes made to the system. This section briefly describes these "major" updates to CMAQ, providing the reader with an understanding of what was updated in the model and why. A comprehensive description of all the updates made in v5.1 and in-depth technical documentation of those changes can be found on the CMAS Center website for the CMAQ v5.1 release at https://cmaswiki-cempd.vipapps.unc.edu/index.php/CMAQ_version_5.1_(November_2015_release)_Technical_Documentation.

2.1 WRF and CMAQ meteorological and transport updates

The WRF and CMAQ models were updated to improve the representation of land-surface processes and vertical mixing. There were two changes made to the PX-LSM in WRF. First, the stomatal conductance function for photosynthetically active radiation (PAR) was revised based on measurements of net photosynthetic rate as a function of PAR for cotton plants reported by Echer and Rosolem (2015). The new functions yield a significantly lower magnitude when short-wave radiation is less than 350 Wm^{-2}. This in turn results in reduced latent heat flux and enhanced sensible heat flux, causing a delay in surface stabilization (prolongs mixing) during evening transitions hours (i.e. sunset). This reduces overestimations (reduced positive bias) in water vapor mixing ratios, which are common in the WRF-CMAQ modeling system during the evening transition. Similarly, overestimation of concentrations of surface emitted species (e.g. NO, NO_2, CO and EC) are also reduced during the evening transition. This change was released in WRFv3.7 and further revised in WRFv3.8. The second change made to the PX-LSM is an increase of the coefficient to the surface energy forcing in the soil temperature force-restore equation (C_v), which is related to volumetric heat capacity (c_v) and heat conductivity (λ) (Pleim and Gilliam 2009) as:

$$C_v = 2\left(\frac{\pi}{c_v \lambda \tau}\right)^{1/2}$$

where τ is 1 day (86400 s), from the previous value of $8x10^{-6}$ K m^2 J^{-1} recommended by Giard and Bazile (2000) to 1.2 $x10^{-5}$ K m^2 J^{-1}. The new value for C_v results from updated values for c_v and λ for vegetation based on measurements of various leaves by Jayakshmy and Philip (2010) (c_v = $2.0x10^6$ J m^{-3} K^{-1}, λ = 0.5 W m^{-1} K^{-1}). These changes reduce overestimations of minimum 2-meter temperature (i.e. warmer surface temperatures) during the early morning (dawn) hours while also reducing underestimations of 2-meter temperature during the post-dawn hours.

There were also two major revisions made to the ACM2 vertical mixing scheme in both WRF and CMAQ. In WRF, the ACM2 was updated to estimate and apply different eddy diffusivities for momentum (K_m) and heat (K_h) so that the Prandtl number (Pr) is no longer assumed to be unity ($Pr = K_m/K_h \neq 1$). The second major modification to ACM2 is the implementation of new stability functions for both heat and momentum for stable conditions, which allows for more mixing in the stable regimes, particularly moderately stable conditions that often occur in the early evening hours. CMAQ v5.1 has also been modified to include the same stability functions that are used in WRF v3.7, and therefore, for consistency, WRF v3.7 (or newer) and CMAQ v5.1 should be used together. Both of these revisions to the ACM2 are described in Pleim et al. (2016).

The Monin-Obukhov length (MOL) values used in the ACM2 model in CMAQ were found to differ from the MOL values used in the ACM2 model in WRF. Specifically, the output from WRF was for a preliminary estimate of MOL that was computed in the surface layer model in WRF (module_sf_pxsfclay.F). The MOL was later re-computed in ACM2 in WRF but not loaded into the output array. This inconsistency has been fixed in v5.1 by re-computing the MOL in CMAQ exactly as it is computed in ACM2 in WRF. However, starting with WRF v3.8, this re-computed MOL value will be available in the WRF output, and therefore it will be unnecessary to re-compute the MOL value in CMAQ.

2.2 Scientific improvements in the CMAQ v5.1 aerosol treatment

CMAQ has historically underestimated SOA in both urban (Woody et al., 2016) and rural (Pye et al., 2015) locations. Thus, improvements to the representation of aerosol from anthropogenic and biogenic hydrocarbons were needed. The updates to SOA formed from anthropogenic volatile organic compounds (VOC) focus on VOC compounds in existing emission inventories, such as the EPA National Emissions Inventory (NEI), that are likely to fall in the intermediate VOC (IVOC) range. These include long-chain alkanes such as heptadecane and polycyclic aromatic hydrocarbons (PAHs) such as naphthalene. Since these compounds are much less volatile than traditional VOCs, they readily form aerosol in high yields. Long-chain alkanes and PAHs were included in other VOC categories in CMAQ versions prior to v5.1, but were lumped with smaller, more-volatile compounds that did not form SOA with the same efficiency. By separating long-chain alkanes and naphthalene at the emission processing step, CMAQ can better account for their higher yields. Several studies (e.g. Pye and Pouliot, 2012; Jathar et al., 2014) have indicated that a large fraction of VOC emissions, particularly IVOC-type compounds, may not be characterized in emission inventories, which limits how much SOA can be formed from anthropogenic VOCs in current chemical transport models.

Several new SOA species were introduced in v5.1 AERO6, specifically AALK1 and AALK2 (from long-chain alkanes) and APAH1, APAH2, and APAH3 (from naphthalene). CMAQ v5.1 predicted alkane SOA is responsible for ~20 to 50% of SOA from anthropogenic VOCs, with the largest absolute concentrations occurring during summer in urban areas. Naphthalene oxidation is predicted to produce more modest amounts of SOA (Pye and Pouliot, 2012). Note that PAH SOA in v5.1 only considers naphthalene as the parent hydrocarbon, which about half of the PAHs is considered as SOA precursors in Pye and Pouliot (2012).

This approach was used since naphthalene is a high priority hazardous air pollutant (HAP) and necessary in the model for purposes other than SOA formation.

CMAQv5.1 has been updated to include the isoprene epoxydiols (IEPOX) SOA resulting from aqueous reactions for most chemical mechanisms including CB05 and SAPRC07 as described in Pye et al. (2013). Later generation isoprene oxidation products formed under low-NO_X conditions, specifically IEPOX, are recognized as a significant source of SOA based on laboratory (Surratt et al. 2010), field (Hu et al. 2015), and modeling (McNeill et al. 2012, Pye et al. 2013, Marais et al. 2016) studies. This SOA is linked to sulfate and acidity and thus represents an anthropogenically controlled source of biogenic SOA.

In addition to the SOA updates for anthropogenic VOCs, $AISO_3$ (acid catalyzed isoprene epoxide aerosol) was also revised in CMAQv5.1 to represent SOA from IEPOX. For the CB05tucl, CB05e51 and SAPRC07 chemical mechanisms with IEPOX formation in the gas-phase, heterogeneous uptake of IEPOX on acidic aerosol results in SOA (Pye et al., 2013). This IEPOX SOA replaces the $AISO_3$ treatment based on Carlton et al. (2010). The AISO3J species name is now retained for IEPOX SOA and represents the sum of IEPOX-derived organosulfates and 2-methyltetrols. Explicit isoprene SOA species including 2-methyltetrols, 2-methylglyceric acid, organosulfates, and oligomers/dimers are available in the SAPRC07tic with AERO6i mechanism now available in CMAQv5.1. See Table 1 for more information regarding these new SOA species.

2.3 Improvements to the CMAQv5.1 in-line photolysis and cloud model

The in-line calculation of photolysis rates in CMAQ has undergone significant changes. The calculation of photolysis rates in v5.1 still uses the same approach for calculating actinic fluxes by solving a two-stream approximation of the radiative transfer equation (Binkowski et al., 2007; Toon et al., 1989) over wavebands based on the FAST-J photolysis model (Wild et al., 2000). Each layer includes scattering and extinction using simulated air density, cloud condensates, aerosols, and trace gaseous such as O_3 and NO_2. The first area changed in v5.1 is how clouds are described in the actinic flux calculation. In v5.0.2, a vertical column had a single cloud deck with constant cloud fraction, liquid water content and water droplets as the source of scattering and extinction from clouds. These cloud parameters were diagnosed from humidity and air temperature predicted by the meteorological model (e.g WRF). CMAQv5.1 uses additional information available from WRF that describes the resolved cloud cover, which allows the vertical column to have multiple cloud decks with variable cloud fractions and multiple types of water condensates. In addition to the resolved cloud cover, v5.1 also includes the radiative effect from CMAQ's sub-grid convective clouds in the calculation of actinix fluxes. CMAQ uses the ACM cloud model to describe sub-grid convective clouds based on convective precipitation rates from WRF. These updates to the clouds used in the photolysis rates improved CMAQ's internal consistency between cloud mixing, aqueous chemistry, and gas-phase chemistry.

The second area of change to the in-line photolysis calculation addressed the radiative effect from aerosols. The mixing model used to compute the refractive indices of aerosol modes (an internal-volume weighted average model) allows the refractive index of each aerosol component to depend on wavelength. Most importantly, the refractive index for elemental (black) carbon reflects the current scientific consensus (Bond and Bergstrom, 2006; Chang and Charalampopoulos, 1990; Segelstein, 1981; Hess et al., 1998) and increases its absorptive capacity from the value v5.0.2. Additionally, estimating aerosol optical properties includes new options to solve Mie scattering theory, or the option to use the Core-Shell model with an elemental carbon core (Bohren and Huffman, 2004). A user can choose to use these options by setting environment variables before executing the CMAQ model (http://www.airqualitymodeling.org/cmaqwiki/index.php?title=CMAQv5.1_In-line_Calculation_of_Photolysis_Rates). By

default, v5.1 uses approximate solutions to Mie scattering and the internal-volume weighted average model (Binkowski et al., 2007). Third, several new variables (e.g. resolved cloud fraction, sub-grid cloud fraction, resolved cloud water content) have been added to the cloud diagnostic file that describe the optical properties of aerosol and clouds and their radiative effects.

2.4 Improvements in CMAQ v5.1 atmospheric chemistry

Several changes were made to the CB05TUCL chemical mechanism in v5.1 (Whitten et al., 2010; Sarwar et al., 2012), which is now referred to as CB05e51. These changes include updates to reactions of oxidized nitrogen (NO_Y) species; incorporation of new research on the atmospheric reactivity of isoprene photo-oxidation products; addition of several high priority HAPs to the standard CB05e51 mechanism (following the protocol in the multipollutant version of CMAQ); and other changes to update the mechanism and make it compatible with updates to the aerosol chemistry, but overall retaining the fundamental core of the CB05 mechanism. A more detailed explanation of the changes made in the CB05e51 mechanism is provided below.

2.4.1 NO_Y updates and additions

The most extensive changes made consisted of updates and extensions of the NO_Y species, including peroxyacylnitrates, alkyl nitrates, and NO_X reactions with HO_X. The thermal formation and degradation of peroxyacetyl nitrate (PAN) were modified to correct the parameters that describe the rate constant pressure dependence in the fall-off region between the high-pressure limit and the low-pressure limit based on the values determined by Bridier et al. (1991). An additional species, MAPAN, was added to explicitly represent PANs from methacrolein because these are a possible contributor to SOA formation. The $OH+NO_2$ reaction rate was updated based on Troe (2012) and a small yield of HNO_3 (<1% at standard temperature and pressure, varying with temperature and pressure) was added to the reaction of HO_2+NO (Butkovskaya et al., 2007). The single alkyl nitrate species in CB05, NTR, was replaced with seven species to better investigate the variety of chemical and physical fates of alkyl nitrates. The first-generation monofunctional alkylnitrates and difunctional hydroxy nitrates were assigned Henry's law constants of 6.5e-1 M and 6.5e3 M respectively, while second generation carbonyl nitrates were assigned 1.0e3 M and multifunctional hydroxynitrates were assigned a value of 1.7e4 M. Five species are predominantly from anthropogenic sources, with the relative distribution of mono-functional (alkyl nitrates) and multi-functional (hydroxy, carbonyl, hydroxycarbonyl, and hydroperoxy) nitrate products determined based on the nitrates produced from the five alkanes and alkenes, with the largest emissions as listed in the NEI (Simon et al., 2010). The other two nitrate species represent first generation and later generation nitrates from biogenic (isoprene and terpene) sources. Biogenic nitrate products were based on reaction products from Lee et al. (2014), with NO_X recycling from secondary biogenic nitrate products (Jenkin et al., 2015) and photolysis rates with quantum yields of unity. Finally, a heterogeneous hydrolysis rate of alkyl nitrates was added (Hildebrandt-Ruiz et al., 2013), with a six-hour lifetime on aerosol at high relative humidity (Liu et al., 2012; Rollins et al., 2013). Additional details can be found in the CMAQv5.1 release documentation (http://www.airqualitymodeling.org/cmaqwiki/index.php?title=CMAQ_version_5.1_(November_2015_release)_Technical_Documentation).

2.4.2 Other changes

The high HO_X pathways for isoprene oxidation have been modified to explicitly account for production of IEPOX, which can form SOA and modify the gas-phase concentrations. The high NO_X pathways have been modified to explicitly produce methacrolein PAN (MAPAN, described in Section 2.4.1) because it reacts faster with OH than other PAN species. Several high priority HAPs were added to the standard version of CB05e51 as either active species or reactive tracers, specifically acrolein, 1,3-butadiene

(which produces acrolein), toluene, xylene isomers, α- and β-pinene, and naphthalene using reaction pathways and rates as defined by IUPAC. Refer to the CMAQv5.1 release documentation for additional details on these updates.

Several other, smaller changes were made to the chemistry to either improve consistency with IUPAC, enhance the integration with heterogeneous chemistry, or for numerical consistency. These include the updates to the products of ethanol reaction with OH using recommended yields from IUPAC (http://iupac.pole-ether.fr; accessed May 11, 2016); updates to the reactions of acylperoxy radicals with HO_2 to include a 44% yield of OH; the addition of a new species, SOAALK, to account for SOA formation from alkanes; and the addition of gas-phase and heterogeneous nitryl chloride formation ($ClNO_2$) and $ClNO_2$ photolysis as described by Sarwar et al. (2012).

2.5 Updates to air-surface exchange processes in CMAQ v5.1

Meteorologically dependent emissions and deposition, hereafter referred to as air-surface exchange, were extensively updated in v5.1. A data module was developed to share meteorological and calculated atmospheric transport environmental variables between vertical diffusion, deposition, and meteorological dependent emissions to more consistently represent processes common to both deposition and emissions. Additionally, sea salt and biogenic emissions and dry deposition routines were updated.

2.5.1 Sea salt aerosol emission

The sea salt aerosol emissions module was updated to better reflect emissions estimates from recent field observations and to incorporate ocean thermodynamic impacts on emissions. The size distribution of sea salt aerosol was expanded to better reflect recent fine-scale aerosol measurements in laboratory and field studies (de Leeuw et al., 2011) by modifying the Θ parameter of Gong (2003) from 30 to 8. A sea-surface temperature (SST) dependency to the sea-salt aerosol emissions following Jaeglé et al. (2011) and Ovadnevaite et al. (2014) was also added, which increased accumulation and coarse mode sea-salt emissions in regions with high SSTs and reduced the emissions in regions with low SSTs. Finally, the surf-zone emissions of sea-salt aerosol were reduced by 50% assuming a decrease in the surf-zone width from 50 m to 25 m to address a systematic overestimation of near-shore coarse sea-salt aerosol concentrations (Gantt et al., 2015).

2.5.2 Biogenic emissions (BEIS)

There were also several updates to the calculation of non-methane biogenic volatile organic carbon (BVOC) emissions in v5.1. The Biogenic Emissions Inventory System (BEIS; https://www.epa.gov/air-emissions-modeling/biogenic-emission-inventory-system-beis) model was updated to include the implementation of a dynamic two-layer, sun and shaded, vegetation canopy model, while the PAR response function was integrated into the canopy model following Niinemets et al. (2010) for each canopy layer. In earlier versions of BEIS, emissions were a function of the 2-meter temperature which was inconsistent with measured emission factors that were empirically correlated with leaf temperature. BEIS 3.6.1 released with v5.1 was updated to model emissions as a function of the leaf temperature rather than 2-meter temperature to be more consistent with how BVOC emission factors are typically estimated. For additional details see Bash et al. 2016. Finally, the Biogenic Emission Land-use Data (BELD) version 4.0 and emission factors for herbaceous wetlands were updated to address overestimates of BVOCs at coastal sites (Guenther et al., 2006), and the BELD land-use and vegetation species were updated using high-resolution satellite data and in-situ survey observations from 2002-2012 (Bash et al., 2016).

2.5.3 Dry deposition

There were two important updates to the dry deposition calculation in v5.1. First, the dry deposition of O_3 over oceans was updated to include the additional sink due to interaction with iodide in the seawater (marine halogen chemistry), with the iodide concentrations estimated based on sea-surface temperature (Sarwar et al., 2015), which increased the O_3 deposition velocity over oceans. Second, over vegetative surfaces, the wet cuticular resistance was updated following Altimir et al. (2006), 385 s m^{-1}, and dry cuticular resistance was set to the value of Wesley (1989) for lush vegetation, 2000 s m^{-1}. These changes resulted in an approximately 2.0 ppbV reduction in the modeled O_3 mixing ratios, with the largest reductions, ~10%, occurring during the nighttime and early morning hours, and approximately a 2% reduction in the modeled midday O_3 mixing ratio.

2.5.4 Gravitational Settling

Previous evaluations of the ground-level coarse particle (PM_{10}) concentrations in CMAQ have shown that the model significantly underestimated the total PM_{10} concentrations (Appel et al., 2012). Contributing to this underestimation is the fact that CMAQ previously did not have a mechanism in place to allow coarse particles to settle from upper layers to lower layers (although coarse particles in layer one can settle to the surface). As a result, large particles that would normally settle to lower layers in the model could remain trapped in the layers in which they were emitted or formed. To account for this deficiency in the model, the effects of gravitational settling of coarse aerosols from upper to lower layers has been added to v5.1 to more realistically simulate the aerosol mass distribution. The net effect of this update is an increase in ground-level PM_{10} concentrations in v5.1 compared to v5.0.2, particularly near coastal areas impacted by sea-spray (Nolte et al., 2015).

As stated in the beginning of this section, but is useful to reiterate here, the information provided in this section only covers a portion of the vast number of updates that went into v5.1, and was intended to make the reader aware of the more significant changes made and why, but often avoids including the very specific detailed code changes that were made to the model. Those seeking a complete detailed list of all the changes made to the model should refer to the v5.1 technical documentation using the link provided at the beginning of this section.

3 Modeling setup and observational data sets

The modeling setup for the evaluation of v5.1 utilizes a domain covering the entire contiguous United States (CONUS) and surrounding portions of northern Mexico and southern Canada, and the eastern Pacific and western Atlantic oceans. The modeling domain consists of 299 north-south by 459 east-west grid cells utilizing 12-km by 12-km horizontal grid spacing and 35 vertical layers with varying thickness extending from the surface to 50 hPa and an approximately 10-meter mid-point for the lowest (surface) model layer. The simulation time period covers the year 2011, which is a base year for the EPA's NEI and also a period during which specialized measurements from a variety of trace species are available from the Deriving Information on Surface Conditions from Column and Vertically Resolved Observations Relevant to Air Quality (DISCOVER-AQ; http://www.nasa.gov/mission_pages/discover-aq/index.html) campaign.

All the CMAQ simulations presented here employed the Euler Backward Iterative (EBI) solver. The v5.0.2 simulations utilized the windblown dust treatment available, while the v5.1 simulations did not due to errors in the implementation of the windblown dust model in v5.1. However, the overall contribution of windblown dust to $PM_{2.5}$ is small on a seasonal average and does not affect the seasonal comparisons shown in Section 5. Additional details regarding the options employed in the CMAQ simulations are available upon request from the corresponding author. For the annual simulations, a 10-day spin-up period in December 2010

was used (and then discarded) to reduce the effects of the initial conditions, after which the model was run continuously for the entire year 2011 (one continuous simulation stream). For the one-month January and July sensitivity simulations presented, 10-day spin-up periods in the previous month were used and then discarded. Boundary conditions for the 12-km CMAQ simulations are provided by a 2011 hemispheric GEOS-Chem (Bey et al., 2001) with the chemical species mapped to the corresponding CMAQ species.

Several sets of CMAQ simulations were performed to help thoroughly evaluate both the overall change in model performance between v5.0.2 and v5.1 and to examine the individual impact of specific model process changes on the model performance. As such, different input data sets were used/required for the v5.0.2 and v5.1 simulations. The base v5.0.2 simulation (CMAQv5.0.2_Base) utilized WRF v3.4 meteorological input data, while WRF v3.7 derived meteorological data were used for all the v5.1 simulations presented here. As stated previously, different versions of WRF were used for the v5.0.2 and v5.1 simulations due to the updates made in both WRF and CMAQ (Section 2.1) that would have made performing the CMAQ simulations with output from the same version of WRF difficult and introduce some inconsistencies. While there were other updates made to WRF between versions 3.4 and 3.7, those changes were minor and did not impact the WRF results significantly for the configuration of the model used here.

Both WRF simulations employed the same options, which include the Rapid Radiation Transfer Model Global (RRTMG) long and short wave radiation (Iacono et al., 2008), Morrison microphysics (Morrison et al., 2005), and the Kain-Fritsch 2 cumulus parametrization (Kain, 2004). For the LSM and PBL models, the PX-LSM and ACM2 were used. Four-dimensional data assimilation (FDDA) was also employed in the WRF simulations. The namelists used for each WRF simulation are provided in the supplemental material (see S.4 and S.5). Model ready meteorological input files were created using version 4.1.3 of the Meteorology-Chemistry Interface Processor (MCIP; Otte and Pleim, 2010) for the WRF v3.4 data and MCIP version 4.2 (https://www.cmascenter.org/help/documentation.cfm?model=mcip&version=4.2) for the WRF v3.7 data.

Emission input data for the v5.0.2 simulation were based on version 1 (v1) of the 2011 modeling platform developed by the USEPA from regulatory applications (https://www.epa.gov/sites/production/files/2015-08/documents/lite_finalversion_ver10.pdf), while the base v5.1 simulation utilized emission data based on version 2 (v2) of the 2011 modeling platform. The v2 emission data became available after the completion of the v5.0.2 simulation using v1 emission data and it was determined that the latest version of the emission data would be used for the v5.1 simulation in order to obtain the best results. However, based on sensitivity simulations performed for January and July 2011 where the only difference was the emissions platform used, the differences in O_3 and $PM_{2.5}$ between those two simulations used were generally small and isolated, suggesting there is minimal impact to the comparison between the v5.0.2 and v5.1 simulations from the change in the emissions platform used. Figure S1 shows the impact on winter (January) and summer (July) O_3 and $PM_{2.5}$ between simulations using the different emission platforms.

The raw emissions files were processed using versions 3.5 (v1 emissions) and 3.6.5 (v2 emissions) of the Sparse Matrix Operator Kernel Emissions (SMOKE; https://www.cmascenter.org/smoke/) to create gridded, speciated hourly model-ready input emission fields for input to CMAQ. Electric generating unit (EGU) emissions were obtained using data from EGUs equipped with Continuous Emission Monitoring System (CEMS). Plume rise for point and fire sources were calculated in-line for all simulations (Foley et al., 2010; https://www.cmascenter.org/cmaq/documentation/4.7.1/INLINE_EMISSIONS_DEPV_NOTES.txt). Biogenic emissions were generated in-line in CMAQ using BEIS versions 3.14 for v5.0.2 and 3.61 (Bash et al., 2016) for v5.1. All the

simulations employed the bi-directional ammonia flux (bi-di) option for estimating the air-surface exchange of ammonia, as well as the in-line estimation of NO_X emissions from lightning strikes.

Output from the various CMAQ simulations is paired in space and time with observed data using the Atmospheric Model Evaluation Tool (AMET; Appel et al., 2011). There are several regional and national networks that provide routine observations of gas and particle species in the U.S. The national networks include the EPA's Air Quality System (AQS; 2086 sites; https://www.epa.gov/aqs) for hourly and daily gas and aerosol PM species; the Interagency Monitoring of PROtected Visual Environments (IMPROVE; 157 sites; http://vista.cira.colostate.edu/improve/) and Chemical Speciation Network (CSN; 171 sites; https://www3.epa.gov/ttnamti1/speciepg.html) for daily average (measurements typically made every third or sixth day) total and speciated aerosol PM species; and the Clean Air Status and Trends NETwork (CASTNET; 82 sites; http://www.epa.gov/castnet/) for hourly O_3 and weekly aerosol PM species. In addition to these routinely available observations, the DISCOVER-AQ campaign (https://www.nasa.gov/mission_pages/discover-aq/) during July 2011 provides additional ground-based gas and aerosol PM measurements, along with unique aloft measurements made by aircraft, vertical profilers (e.g. Light Detection And Ranging (LiDAR) measurements), ozonesondes and tethered balloons (not utilized in this analysis however).

4 Evaluation of major scientific improvements

In this section we evaluate the impact that several of the major scientific improvements in v5.1 have on the operational model performance. Unlike Foley et al. (2010), in which several individual major scientific improvements in CMAQ v4.7 were evaluated incrementally (e.g. each subsequent improvement is evaluated against the previous improvement), here we examine each scientific improvement separately by comparing simulations with the specific improvement removed (i.e. as it was in v5.0.2) to the base v5.1 simulation (CMAQv5.1_Base) which includes all the updates. While this has the disadvantage of not showing the incremental change in model performance due to each improvement, it does limit the number of simulations that need to be performed. In addition, it allows for easier examination of the effect of nonlinear increments on total model performance, as some updates to the modeling system may be affected by updates to other parts of the model, the effects of which on model performance may not be captured in an incremental testing format. Note that while some attempt is made to broadly identify the processes involved that cause the observed changes in model performance between v5.0.2 and v5.1, it would be too laborious (both to the reader and to the investigators) to comprehensively describe and investigate in-depth the processes involved that result in each observed difference in model performance described in this section. Where appropriate, the analyses presented in this section use the v5.0.2 base simulation (CMAQv5.0.2_Base) for comparison to the scientific improvement while for other improvements the v5.1 base simulation is used for comparison. In each case, the simulations being compared are noted. Table 2 provides a description of the CMAQ model simulations referred to in the following sections.

4.1 WRF and CMAQ meteorological updates

As discussed in section 2.1, there were several significant corrections/improvements made to the meteorological calculations in both WRF and CMAQ. While the focus of this work is on updates to the CMAQ model, certain options within WRF and CMAQ are linked, and therefore it is necessary to discuss the WRF model updates alongside the corresponding CMAQ model updates.

Figure 1 shows the cumulative impact that all the meteorological changes in WRF and CMAQ (i.e. changes to ACM2 and MOL) had on O_3 and $PM_{2.5}$ in January and July by comparing the CMAQv5.0.2_Base simulation to a CMAQv5.0.2 simulation using

WRFv3.7 (CMAQv5.0.2_WRFv3.7) which includes the ACM2 and MOL updates. The effect of the changes on O_3 in January is mixed, with some areas (e.g. Florida, Chicago and the Northwest) showing a relatively large (2.5 ppbV) increase in O_3, while other areas (e.g. Southwest and Texas panhandle) show a relatively large decrease (-2.5 ppbV) in O_3. For $PM_{2.5}$, the differences in January are generally small and isolated, however there is a relatively large increase in $PM_{2.5}$ (>2.5 μgm^{-3}) in the San Joaquin Valley (SJV) of California due to the updates, which combined with the decrease in O_3 there as well, indicates a likely reduction in PBL height and mixing as the cause. There are also some relatively large decreases (1.5 – 2.0 μgm^{-3}) in $PM_{2.5}$ in the Northeast and around in the Great Lakes region (i.e. Chicago). Otherwise, most of the remaining impacts on $PM_{2.5}$ are relatively small (< 1.0 μgm^{-3}).

For July, the meteorological updates in WRF and CMAQ result in exclusively increased O_3 mixing ratios over land, which are considerably larger than the impacts observed in January. The largest increases (4.0 – 10.0 ppbV) occur in the eastern U.S., particularly in the Southeast. Smaller increases of 2.0-4.0 ppbV occur across much of the U.S., while in the Gulf of Mexico and the Caribbean O_3 mixing ratios decrease roughly 2.0 – 6.0 ppbV across a large area. The difference in $PM_{2.5}$ in July is similar to that in January, with mostly small, isolated increases or decreases occurring in the eastern U.S. The largest increase (2.0 – 2.5 μgm^{-3}) occurs in the southern Ohio Valley (Kentucky and West Virginia), while the largest decreases (> 2.5 μgm^{-3}) occur in Louisiana and Texas (i.e. Houston).

It makes intuitive sense to see summertime O_3 mixing ratios increasing due to the meteorological changes in WRF and CMAQ, since the net effect of those changes was to increase mixing, particularly in the late afternoon and early evening, which in turn decreases the amount of NO titration of O_3 that occurs in the model, and ultimately results in higher O_3 mixing ratios on average. Conversely, $PM_{2.5}$ concentrations would be expected to decrease due to the increased mixing in the model, which would effectively decrease the concentrations of primary emitted pollutants (e.g. EC and OC), which was observed in areas with the largest emissions (i.e. urban areas). In addition, changes in the oxidant (i.e. OH) concentrations would also potentially affect $PM_{2.5}$ concentrations through increased or decreased SOA formation (spatial heterogeneity of $PM_{2.5}$ formation) which results in spatially varying increases and decreases in $PM_{2.5}$ concentrations.

4.2 Aerosol updates

Several new SOA species from anthropogenic VOCs (i.e. AALK1, AALK2, APAH1, APAH2 and APAH3; Table 1) were added to AERO6 in v5.1 that were not present in v5.0.2. Figure 3 shows the difference in the monthly average sum total concentration of these five species for January and July 2011 between the CMAQv5.0.2_Base and CMAQv5.1_Base simulations. Since none of these species were present in v5.0.2, the difference totals in Figure 2 represent the additional SOA mass that these five species contribute to the total $PM_{2.5}$ mass in v5.1. For both January and July, the monthly average concentration of these species is small, ranging between 0.0-0.1 μgm^{-3}, with the largest concentrations in the eastern half of the U.S., particularly in the upper Midwest. However, the concentration of these new species during shorter time periods and smaller, isolated regions would be larger. In addition, the inclusion of these new species is potentially important for health related studies on the impact of PAHs. Overall however, these new species represent a small addition to the total $PM_{2.5}$ concentration in the model.

Along with the introduction of the new SOA species above, the pathways for the formation of acid enhanced isoprene SOA were also updated. The bottom panels in Figure 2 show the monthly average difference in the sum of the species containing isoprene SOA (AISO1, AISO2, AISO3 and AOLGB) between v5.1 and v5.0.2 (v5.1 – v5.0.2). For January, the difference in the sum of

these species is relatively small, with minimum and maximum values peaking around ±0.5 μgm^{-3} consistent with the fact that isoprene emissions are low in winter. For July the difference is always positive (v5.1 higher than v5.0.2) and much larger compared to January, with peak differences exceeding 2.5 μgm^{-3}, primarily in the areas with the highest aerosol SO_4^{2-} concentrations (i.e. Ohio Valley). Therefore, the updated IEPOX-SOA formation pathways in v5.1 represent a potentially significant contribution to the total $PM_{2.5}$, particularly during the summer. Increased isoprene emissions in v5.1 with BEIS v3.61 compared to v5.0.2 with BEIS v3.14 also contribute to the larger contribution of isoprene SOA in v5.1.

4.3 Cloud model and in-line photolysis updates

Changes in the photolysis/cloud model treatment in v5.1 have potentially significant impacts on the O_3 and $PM_{2.5}$ estimates from the model. Figure 3 shows the difference in O_3 and $PM_{2.5}$ for the CMAQv5.1_Base simulation and the CMAQv5.1_RetroPhot simulation (see Table 2 for simulation description). The CMAQv5.1_RetroPhot simulation is the same as the CMAQv5.1_Base simulation except it employs the same (old) photolysis/cloud model treatment as in v5.0.2. For January, O_3 mixing ratios (Figure 3a) and $PM_{2.5}$ concentrations (Figure 3c) are both higher across the Southeast and portions of California in the v5.1 simulation, indicating that v5.1 has much less photolysis attenuation due to the updates in the representation of cloud effects on photolysis.

The impact of the updated photolysis in v5.1 is considerably larger in July (when there is more convection) than in January. Peak O_3 differences in January were around 2.0 ppbv, whereas in July peak differences of greater than 5.0 ppbv (Figure 3b) occur over the Great Lakes (where low PBL heights can enhance the impact of changes in O_3). However, in general the difference in O_3 mixing ratios is larger in both magnitude and spatial coverage in July compared to January, indicating that the updated photolysis/cloud model treatment in v5.1 increases O_3 to a greater extent in July compared to January, as expected due to increased photolysis rates in the summer compared to winter. Overall, differences in O_3 in July range on average from 1.0 to 3.0 ppbv, with larger differences occurring in the major urban areas (e.g. Atlanta, Charlotte and Los Angeles) and off the coast of the Northeast corridor. The change in $PM_{2.5}$ is also larger (both in magnitude and spatial coverage) in July than January (Figure 3d). The greatest change is primarily confined to the eastern U.S., resulting in a roughly 0.1 to 0.5 μgm^{-3} increase in $PM_{2.5}$ in v5.1, with the maximum increase located over the Great Lakes region and areas to the south, the result of increased SOA and gas-phase production of SO_4^{2-} due to greater OH^- concentrations in v5.1.

Additional diagnostic evaluation of photolysis/cloud model treatment in CMAQ was conducted based on the model predicted cloud albedo at the top of the atmosphere. The predicted cloud albedo from WRFv3.7, CMAQv5.0.2 and CMAQv5.1 were evaluated against cloud albedo from NASA's Geostationary Operational Environmental Satellite Imager product (GOES; http://satdas.nsstc.nasa.gov/). This evaluation was used to qualitatively determine if one CMAQ version better considers how clouds affect calculated photolysis rates. The GOES product has a 4km horizontal resolution and was re-gridded to the 12-km grid structure used in the WRF and CMAQ simulations using the Spatial Allocator utility (https://www.cmascenter.org/sa-tools/). The satellite data are available at 15 minutes prior to the top of the hour during daytime hours and were matched to model output at the top of the hour (see section S.1 in the supplemental material for further information). Figure 4 shows the average cloud albedo or reflectivity at the top of the atmosphere during daytime hours in July 2011 derived from the GOES satellite product (Figure 4a), and the cloud parameterizations within: WRF3.7 (Figure 4b), CMAQv5.1_RetroPhot (Figure 4c) and CMAQv5.1_Base (Figure 4d). Comparison of Figure 4b to 4c shows the dramatic differences between the clouds predicted by WRFv3.7 and the predictions from the cloud parameterization in v5.0.2. Most of these large differences, particularly over

land, are now gone in model predictions from the CMAQv5.1_Base simulation which uses resolved clouds from WRF and sub-grid clouds from the convective cloud model within CMAQ (compare Figure 4b to 4d).

Two notable issues remain with the v5.1 modeled cloud parametrization. The photolysis cloud parameterization in v5.1 produces more clouds over water compared to the WRF parameterization, which is itself biased high for some parts of the Atlantic Ocean compared to GOES. This issue will be addressed by science updates planned for the CMAQ system and evaluation results are expected to improve in the next CMAQ release. A more significant issue, from an air quality perspective, is the under-prediction of clouds over much of the Eastern and West Central U.S. in the WRF predicted clouds, which is now directly passed along to CMAQ. This misclassification of modeled clear sky conditions can contribute to an over prediction of O_3 in these regions. Resolving this issue will require changes to the WRF cloud parameterization. Future research will also include changing the sub-grid cloud treatment currently used in the CMAQ system to be consistent with the sub-grid parameterization used in WRF. Section S.1 in the supplemental material provides a table with additional evaluation metrics of the modeled clouds over oceans versus over land and also describes how cloud albedo was calculated for the three model simulations.

4.4 Atmospheric chemistry updates

As detailed in section 2.4, numerous updates were implemented in the representation of atmospheric chemistry in v5.1. It would be extremely cumbersome to attempt to isolate the impact of each chemistry update individually. Instead, in order to assess the overall impact that the combined chemistry changes have on the model results, model comparisons are conducted using the CMAQv5.1_Base simulation, which employs the CB05e51 chemical mechanism (the v5.1 default chemical mechanism) and the CMAQv5.1_TUCL simulation (see Table 2 for description). The CMAQv5.1_TUCL simulation is the same as the CMAQv5.1_Base simulation except that it employs the CB05TUCL chemical mechanism (Whitten et al., 2010; Sarwar et al., 2012), the default mechanism in v5.0.2. Note that the aerosol updates discussed in section 4.2 were incorporated into the CB05e51 chemical mechanism (in the past that portion of the aerosol chemistry was separate from the gas-phase chemical mechanism). As such, differences between the CMAQv5.1_TUCL and CMAQv5.1_Base simulations include impacts from those changes (i.e. Figure 2). In order to isolate primarily just the effect on $PM_{2.5}$ from the atmospheric chemistry changes, the organic matter (AOMIJ; See S.2 and S.3 for species definition descriptions) mass has been removed from the comparisons of total $PM_{2.5}$ mass discussed below.

Figure 5 shows the difference in monthly average O_3 and $PM_{2.5}$ for January and July between the CMAQv5.1_Base and CMAQv5.1_TUCL simulations. For January, O_3 mixing ratios are higher in the simulation using the CB05e51 mechanism (CMAQv5.1_Base simulation), however the overall impact of CB05e51 on O_3 is generally small (~2-4%), with maximum differences of only approximately 1.0 ppbV (~6%), primarily along the southern coastal areas of the U.S. $PM_{2.5}$ is also higher in January in the simulation using the CB05e51 mechanism (CMAQv5.1_Base simulation), with the largest changes in $PM_{2.5}$ of 0.2 – 0.4 μgm^{-3} (~2-6%) primarily occurring in the eastern U.S. and greater than 1.0 μgm^{-3} (~6-8%) in the SJV of California.

For July, O_3 mixing ratios are higher across most areas in the CMAQv5.1_Base simulation, primarily across northern portions of the U.S., the Great Lakes region and in California (i.e. Los Angeles and the SJV). Most increases in O_3 in the CMAQv5.1_Base simulation range between 0.6 and 1.2 ppbV (~2-4%), however larger increases of over 3.0 ppbV (~4-8%) occur in southern California and over Lake Michigan (likely influenced in-part by low PBL heights over the lake). A small area of lower O_3 mixing

ratios occurs off the eastern coast of the U.S. For July, the difference in $PM_{2.5}$ due to the CB05e51 chemical mechanism is relatively small, with differences in concentrations generally ranging from ±0.50 μgm^{-3} (~2-4%) across the eastern U.S.

5 Evaluation of CMAQv5.1

In this section, comparisons are made of the performance of the CMAQv5.0.2_Base and CMAQv5.1_Base simulations by initially comparing the simulations to each other (model to model) and then evaluating them against a wide variety of available air quality measurements (see section 3). Several common measurements of statistical performance are used, namely mean bias (MB), mean error (ME), root mean square error (RMSE) and Pearson correlation. Note that representativeness (incommensurability) issues are present whenever gridded values from a deterministic model such as CMAQ are compared to observed data at a particular point in time and space, as deterministic models calculate the average outcome over a grid for a certain set of given conditions, while the stochastic component (e.g. sub-grid variations) embedded within the observations cannot be accounted for in the model (Swall and Foley, 2009). These issues are somewhat mitigated for networks that observe for longer durations, for example the CSN and IMPROVE networks which are daily averages and the CASTNET observations which are weekly averages. The longer temporal averaging helps reduce the impact of stochastic processes, which can have a large impact on shorter (e.g. hourly) periods of observation (Appel et al., 2008).

There are several important differences to keep in mind between the comparison of the CMAQv5.0.2_Base and CMAQv5.1_Base simulations beyond the obvious changes to the model process representations discussed in the previous sections. First, the simulations use different versions of WRF (as discussed in Sections 2.2 and 4.1). This was intentional, as it was determined that the changes made from WRF v3.4 (used in the CMAQv5.0.2_Base simulation) to WRF v3.7 (used in the CMAQv5.1_Base simulation) and subsequent required changes made to the CMAQ code represent a change to the overall WRF-CMAQ modeling system and therefore should be evaluated together. Second, the emission inventories for the two base runs are slightly different, as discussed in Section 3. While the changes between the emission inventories are generally minor, they do represent another difference between the simulations, and where possible the effect of the different inventories on the model performance is noted. Finally, it should also be noted that the windblown dust treatment was employed in the CMAQv5.0.2_Base simulation but not in the CMAQv5.1_Base simulation. This was due to issues with the implementation of the updated windblown dust treatment in v5.1 that were not discovered until after the model was released and the CMAQv5.0.2_Base simulation was completed. However, the contribution of windblown dust to total $PM_{2.5}$ in v5.0.2 tends to be small and episodic and therefore should not constitute a significant impact to the performance differences between v5.0.2 and v5.1, especially for the monthly averages generally shown here. For reference, the v5.0.2 simulated seasonal average values of $PM_{2.5}$ and maximum daily 8-hr average (MDA8) O_3 are provided in Figures S2 and S3 respectively.

5.1 $PM_{2.5}$

Figure 6 shows the seasonal average difference in model simulated $PM_{2.5}$ between v5.0.2 and v5.1 (CMAQv5.1_Base – CMAQv5.0.2_Base), with cool colors indicating a decrease in $PM_{2.5}$ in v5.1 (versus v5.0.2) and warm colors indicating an increase in $PM_{2.5}$. Figure 7 shows the seasonal mean bias (MB) for $PM_{2.5}$ for the CMAQv5.1_Base simulation, while Figure 8 shows the change in the absolute value of the seasonal mean bias (|MB|) in $PM_{2.5}$ between the CMAQv5.0.2_Base and CMAQv5.1_Base simulations. Cool colors indicate smaller $PM_{2.5}$ |MB| in the CMAQv5.1_Base simulation (versus the CMAQv5.0.2_Base simulation), while warm colors indicate larger |MB| in the CMAQv5.1_Base simulation.

During winter, v5.1 predicts lower $PM_{2.5}$ concentrations in the eastern U.S. and portions of western Canada compared to v5.0.2, but higher $PM_{2.5}$ concentrations in the SJV and isolated portions of Mexico and Alabama (due to emissions) (Figure 6). Almost all the differences in $PM_{2.5}$ are due to changes in the emissions between the two simulations (see Figure S1a). $PM_{2.5}$ is largely overestimated in the eastern U. S. and underestimated in the western U.S. in the winter in CMAQv5.1_Base simulation (Figure 7a). The change in |MB| between v5.0.2 and v5.1 is negative (reduced MB in v5.1) across the majority of the sites, with relatively large reductions (3-5 μgm^{-3}) in |MB| in the Northeast, upper Midwest (i.e. Great Lakes region), SJV, and portions of the mid-Atlantic (e.g. North Carolina) (Figure 8a). Alabama is a notable exception, with the MB increasing in the v5.1 simulation due to changes in the emissions inventory. Figure S4 presents a histogram of the change in $PM_{2.5}$ |MB| using the same data and color scale as in Figure 8. It's clear from the histogram the large percentage (69.2%) of sites where the |MB| decreases in the v5.1 simulation in the winter (Figure S4a), demonstrating a significant improvement in the $PM_{2.5}$ performance for v5.1 versus v5.0.2.

The diurnal profile of $PM_{2.5}$ for winter (Figure 9a) shows a relatively large decrease in MB throughout most of the day in the v5.1 versus v5.0.2, particularly during the overnight, morning and late afternoon hours. A similar improvement is seen in the RMSE, while the correlation also improves for all hours (Figure S5). Figure 10 shows seasonal and regional stacked bar plots of $PM_{2.5}$ composition (SO_4^{2-}, NO_3^-, NH_4^+, EC, OC, soil, NaCl, NCOM, and Other). Soil is based on the IMPROVE soil equation and contains both primary and secondary sources of soil (Appel et al., 2013), while Other represents the unspeciated PM mass in the inventory (see Appel et al., 2008) The five regions shown in Figure 10 are Northeast (Maine, New Hampshire, Vermont, Massachusetts, New York, New Jersey, Maryland, Delaware, Connecticut, Rhode Island, Pennsylvania, District of Columbia, Virginia and West Virginia), Great Lakes (Ohio, Michigan, Indiana, Illinois and Wisconsin), Atlantic (North Carolina, South Carolina, Georgia and Florida), South (Kentucky, Tennessee, Mississippi, Alabama, Louisiana, Missouri, Oklahoma and Arkansas) and West (California, Oregon, Washington, Arizona, Nevada, New Mexico). These regions are derived from principle component analysis to group states with similar $PM_{2.5}$ source regions together. For winter, the total $PM_{2.5}$ high bias is reduced across all five regions, with most of the improvement coming from primary emitted species such as EC and OC, non-carbon organic matter (NCOM; S.2 or S.3) and Other, indicating that improvements in the representation of mixing under stable conditions helped in reducing the high bias. Still, a large bias remains for OC, which may be due to an overestimation of the residential wood combustion in the NEI.

For spring, the changes in $PM_{2.5}$ are much more isolated than in winter (Figure 6b), with the largest decreases occurring around Montreal (Canada), North Carolina, and portions of the desert Southwest (lack of wind-blown dust in v5.1 likely contributes to this decrease in the desert Southwest). A small increase in $PM_{2.5}$ is again noted in Alabama due to emissions changes between the v1 and v2 emissions. The MB for $PM_{2.5}$ in the spring is relatively small, with most sites having an underestimation of 1-3 μgm^{-3}, while some overestimations of $PM_{2.5}$ occur in the Northeast, Great Lakes and Northwest coast (Figure 7b). As expected with the relatively small changes in $PM_{2.5}$ concentrations in spring, the difference in |MB| between v5.0.2 and v5.1 is relatively small, with most differences in |MB| less than ± 1.0 μgm^{-3} (Figure 8b). Some slightly larger decreases in |MB| occur in the Northeast and Alabama, while some larger increases in |MB| occur in the desert Southwest. About half (49.8%) of the sites show an improvement in |MB| (Figure S3b). The diurnal profile of $PM_{2.5}$ for spring shows a consistent underestimation of $PM_{2.5}$ throughout most the day in the v5.0.2 simulation, which becomes larger in the v5.1 simulation with the overall decrease in $PM_{2.5}$ in the spring (Figure 9b). However, the RMSE is lower during the overnight, morning and afternoon hours in the v5.1 simulation, while the correlation also improves throughout most of the day, the exception being 1pm to 4pm LST (Figure S6). Total $PM_{2.5}$ MB improves in three of the five regions shown in Figure 10, with most of the improvement again coming from reductions in the primary emitted species.

In the summer, $PM_{2.5}$ is considerably higher (> 5.0 μgm^{-3}) across the eastern U.S. in the CMAQv5.1_Base simulation, particularly in Mississippi, Alabama, Georgia and portions of the Ohio Valley, while $PM_{2.5}$ is lower in isolated areas in eastern North Carolina, Montreal, Canada and small areas in the southwest U.S. and Mexico (Figure 6c). The changes in $PM_{2.5}$ in Alabama, Montreal and eastern North Carolina are all related, at least in part, to changes in the emissions between v1 and v2 (see Figure S1b). The increase in $PM_{2.5}$ is primarily due to the updates to the IEPOX-SOA chemistry in v5.1 (Figure 2), updates to BVOC emissions in BEIS v3.61 (approximately 1.0 μgm^{-3} increase $PM_{2.5}$ in the southwest U.S.), and the ACM2/MOL updates in WRF and CMAQ (Figure 1), with smaller contributions from the updates in CB05e51 chemical mechanism (Figure 5) and updates to the clouds/photolysis (Figure 3). Despite the increase in $PM_{2.5}$ with v5.1, $PM_{2.5}$ remains largely underestimated in the summer, with largest underestimations in the southeast U.S. and California (Figure 7c). However, the result of the widespread increase in $PM_{2.5}$ in the CMAQv5.1_Base simulation is a similar large, widespread reduction in the |MB| across the eastern U.S., particularly in the Southeast (except eastern North Carolina and Florida) and the Ohio Valley, where reductions in |MB| range from 3.0 - 5.0 μgm^{-3} (Figure 8c). Smaller increases in the |MB| (typically less than 2.0 μgm^{-3}) occur in eastern North Carolina and Florida, and isolated areas in the western U.S. Of all the sites, 60.4% showed an improvement in |MB|, with a large number of sites showing reductions in |MB| greater than 5.0 μgm^{-3} (Figure S3c). $PM_{2.5}$ is underestimated throughout the day in both the v5.0.2 and v5.1 simulations (Figure 9c) in summer, with the underestimation improving slightly in v5.1, particularly during the afternoon and overnight hours. RMSE improves during the daytime hours in v5.1, while correlation is significantly higher in v5.1 than v5.0.2 throughout the entire day (Figure S7). Total $PM_{2.5}$ is underestimated by the model in four of the five regions (West region being the exception), but improves in three of those four regions with v5.1, with small increases in SO_4^{2-} and NH_4^+, and larger increases in OC and NCOM contributing to the improvement (Figure 10).

For the fall, the difference in $PM_{2.5}$ between v5.0.2 and v5.1 is again small (very similar to the spring), with the largest increases occurring in Alabama and western Canada (both emissions related) and the largest decreases occurring in Montreal, Mexico and isolated areas in the eastern and Midwest U.S. (Figure 6). The overall pattern in MB is somewhat similar to that of the spring (Figure 7d), with relatively small MBs in the Eastern U.S. (±2.0 μgm^{-3}) and larger MBs along the west coast (underestimated in California and overestimated in the Northwest). As expected, the change in the |MB| between v5.0.2 and v5.1 is also relatively small in the fall, with the majority of the sites having a change in |MB| of less than ±2.0 μgm^{-3} (Figure 8d), while 65.3% of the sites show a reduction in |MB| (Figure S7d). The average diurnal profile of $PM_{2.5}$ in the fall (Figure 9d) is similar to the spring, with improved MB in v5.1 during the overnight, morning and late afternoon/evening hours and lower RMSE and higher correlation throughout the entire day (Figure S8). Total $PM_{2.5}$ is overestimated in all five regions in the fall (Figure 10), but improves in v5.1 in four of those regions (exception being the South), with decreases in the primary emitted species responsible for most of the improvement.

5.2 Ozone

For the winter, O_3 widely decreases in the CMAQv5.1_Base simulation versus the CMAQv5.0.2_Base simulation across the western U.S., with the seasonal average decreases ranging between 1.0 – 3.0 ppbV, and several areas where decreases exceed 3.0 ppbV, primarily over the oceans (Figure 11a). In the eastern U.S., the change in O_3 is relatively small and isolated, the exception being along the coast of Louisiana (due to differences in emissions; see Figure S1c) and a small portion of Florida, where increases in O_3 exceed 5.0 ppbV. Ozone is underestimated at most sites across the northern portion of the U.S., with the largest underestimations occurring in Colorado, Wyoming and Utah. Despite the decreases in O_3 with v5.1, O_3 is still overestimated in

Florida, along the Gulf Coast of Mexico, the Southwest U.S. and in California (Figure 12a). There is a widespread reduction in the O_3 |MB| in California and increased |MB| in the upper Midwest with v5.1, while across the rest of the domain the change in |MB| is relatively small and mixed in direction (Figure 13a). The majority of the change in O_3 falls between ±5.0 ppbV, with slightly more sites (55.8%) showing a reduction than increase in |MB| (Figure S9a). The average diurnal profile of O_3 in the winter (Figure 14a) shows slightly lower mixing ratios during most of the day, the exception being the late afternoon and early evening hours when mixing ratios are slightly higher. The result is reduced MB and RMSE, and higher correlation throughout the day with v5.1 versus v5.0.2 (Figure S10). The NO_X diurnal profile also generally improves throughout the day in winter (Figure 15a), with decreased MB and RMSE in the afternoon/early evening and increased correlation throughout the day (Figure S11).

The pattern of change in O_3 between v5.0.2 and v5.1 in spring is similar to winter, with lower O_3 mixing ratios in the western U.S. and higher mixing ratios in the eastern U.S. in v5.1 compared to v5.0.2 (Figure 11b). Decreases in O_3 mixing ratios in the western U.S. in v5.1 range from roughly 1.0 – 3.0 ppbV (similar to winter), while in the eastern U.S. the increases generally range from 1.0 – 2.0 ppbV, with isolated areas of larger increases. The MB of O_3 for the v5.1 simulation primarily ranges from slightly over- to slightly underestimated across most the sites, with larger overestimations along the Gulf Coast and larger underestimations in the western U.S. (Figure 12b). The change in |MB| between v5.0.2 and v5.1 shows mixed results (Figure 13b), with slight increases and decreases across much of the eastern U.S. and a relatively large increase in |MB| in the Midwest (Colorado and Wyoming). The |MB| mostly improved across the Gulf Coast and in California due to reduced O_3 mixing ratios from the new marine halogen chemistry and enhanced O_3 deposition to ocean surfaces. Roughly half (49.4%) of the sites showed a reduction in |MB| (Figure S6b) with v5.1. The diurnal profile of O_3 for spring (Figure 14b) shows a relatively large increase in mixing ratios in the late afternoon and evening (4pm to 10pm LST), resulting in a large improvement in MB during that time (Figure S12). Similar improvements are noted in RMSE and correlation in the afternoon and evening hours. The NO_X diurnal profile also shows a large decrease in the late afternoon and early evening mixing ratios (Figure 15b), with a large decrease in both MB and RMSE during that time, and improved correlation throughout the day (Figure S13).

For the summer, the pattern of change in O_3 is markedly different from the winter and spring, with widespread, large increases in O_3 mixing ratios across the eastern U.S. and decreases in the Gulf of Mexico (partially due to differences in emissions; see Figure S1d), southern Florida and over the eastern Atlantic (Figure 11c) ocean. Increases in O_3 in the eastern U.S. range from 2.0 – 10.0 ppbV, with isolated areas of larger increases in the major urban areas (e.g. Chicago, Illinois and Atlanta, Georgia) that can largely be attributed to the updates to the ACM2 and the MOL calculation in WRF and CMAQ (Figure 2b) as well as increased photolysis in v5.1 versus v5.0.2 (Figure 1). Smaller increases in O_3 occur in the western U.S., particularly southern California and the SJV. Decreases in O_3 over the oceans are also large as a result of the inclusion of marine halogen chemistry in v5.1, with some decreases exceeding 10.0 ppbV. The MB of O_3 for the v5.1 simulation shows widespread overestimations in the eastern U.S., particularly along the Gulf of Mexico, while in the western U.S. the MB is mixed, with the largest overestimations occurring along the California coast (Figure 12c).

As expected, the consequence of the widespread increase in O_3 in the eastern U.S. in v5.1 is a corresponding widespread increase in the |MB| compared to v5.0.2, particularly in the Mid-Atlantic and Southeast (Figure 13c). Ozone |MB| decreases along the coast of Florida and along the Gulf of Mexico, the result of decreased O_3 over the water. The change in |MB| in the western U.S. is mixed, with some areas showing improved |MB| (e.g. SJV), while others show increased |MB| (e.g. southern California). The diurnal profiles of O_3 show that mixing ratios increase throughout most of the day in v5.1 (exception being 12am – 5am) (Figure

14c), resulting in increased MB and RMSE throughout the morning and early afternoon hours (Figure S14). However, RMSE decreases substantially during the late afternoon and overnight hours, and the correlation improves throughout the entire day. The NO_X concentrations are lower throughout the day with v5.1 compared to v5.0.2 (Figure 15c), which results in large improvements in the MB in the morning and afternoon periods and slightly increased MB in the middle of the day, while RMSE and correlation improve throughout the day (Figure S15).

For the fall, the pattern of change in O_3 for v5.1 versus v5.0.2 is nearly identical to spring (Figure 11d), with widespread decreases in O_3 in the western U.S. (possibly due to reduced cloud mixing and entrainment from the free troposphere) and mostly small increases in O_3 in the eastern U.S., with the exception of larger increases in several of the major urban areas (e.g. St. Louis, Missouri and Atlanta, Georgia). The changes are generally small, between ±2.0 ppbV, with isolated areas of larger increases or decreases. Ozone is also lower over the Pacific and Atlantic oceans and the Gulf of Mexico. While the change in O_3 between v5.0.2 and v5.1 very similar to the spring, the MB pattern for v5.1 is not. Unlike the spring where O_3 was largely underestimated, in the fall O_3 is overestimated across most of the sites, much like the summer (Figure 12d). The Midwest sites have lowest overall MB, while the east and west coasts show large overestimations of O_3. The increased O_3 in the eastern U.S. with v5.1 results in generally higher |MB| compared to v5.0.2, while in the western U.S. the result is slightly lower |MB| on average, the exception being southern California (Figure 13d). As was the case in the spring, slightly less than half the sites (48.9%) show a reduction in |MB|, with the majority of the change falling between ±5.0 ppbV (Figure S6d). The diurnal profile of O_3 in the fall shows increased mixing ratios in v5.1 during the daytime hours and slightly decreased mixing ratios overnight (Figure 14d), resulting in increased MB during the daytime and lower MB overnight. However, the RMSE is lower and the correlation is higher throughout the day (Figure S16). Similar to the other seasons, the diurnal profile of NO_X in the fall shows lower mixing ratios throughout the day (Figure 15d), particularly in the early morning and late afternoon hours, resulting in higher MB in the morning and lower MB in the afternoon, while RMSE is lower and correlation is higher throughout the entire day with v5.1 (Figure S17).

5.3 ANs, PNs and NO_Y

Previous studies have shown that CMAQ can significantly overestimate NO_Y mixing ratios (e.g. Anderson et al., 2014). To help address the NO_Y overestimation in CMAQ, updates were made to the atmospheric chemistry in v5.1 pertaining to the formation and cycling of alkyl nitrates (ANs), peroxy nitrates (PNs) and NO_Y in the model (Section 2.4.1). Overall, monthly average hourly NO_Y mixing ratios at AQS sites decreased between approximately 13% (January) and 21% (July) in the CMAQv5.1_Base simulation versus the CMAQv5.0.2_Base simulation. The result is a slight decrease in the normalized mean error (NME) in January from 70% (v5.0.2) to 61% (v5.1), but a much larger decrease in NME in July from 151% (v5.0.2) to 101% (v5.1). Mixing ratios of ANs and PNs are not routinely measured, however the DISCOVER-AQ campaign (https://www.nasa.gov/mission_pages/discover-aq/) that took place over the Baltimore, Maryland and Washington, D.C. area in July 2011 provides aircraft measurements of PNs and ANs, along with NO_2, NO_Y, HNO_3 and O_3 . The National Oceanic and Atmospheric Administration (NOAA) P3B aircraft performed measurement flights on a number of days during the DISCOVER-AQ campaign. Those flights included vertical spirals over several locations, one of which was Edgewood, MD (39.41°N, 76.30°W; 11m above sea level), a site that often measures very high O_3, and in recent years has measured some of the highest O_3 in the eastern U.S.

Figure 16 shows vertical profiles of observed and CMAQ (v5.0.2 and v5.1) simulated O_3, NO_2, NO_Y, ANs, PNs and nitric acid (HNO_3) for the Edgewood site on July 5, 2011. Several spirals were performed over the Edgewood site that day, roughly taking

place in the late morning, early afternoon and late afternoon, so the profiles shown represent an average profile throughout the day. While O_3 is underestimated throughout the PBL by both versions of the model on that day, the underestimation improves significantly in the v5.1 simulation. NO_2 and NO_Y are overestimated throughout the PBL by both versions of the model, but again, the overestimation is greatly improved in the v5.1 simulation. The PNs, ANs, and HNO_3 show mixed results, with the ANs performance improving, the PNs performance degrading and the HNO_3 performance relatively unchanged with v5.1. Note that there has been an update in the recommended PAN formation and degradation equilibrium constant (http://iupac.pole-ether.fr) which lowers the predicted PAN concentrations in CMAQ and is currently being examined for its impact on other species. On this particular day, v5.1 generally shows a large improvement in performance over v5.0.2, however the results on other days may be different, but it does highlight the large change in NO_Y mixing ratios that can be expected with v5.1.

6 Modeled Response to Emission Changes

One of the primary applications of air quality models is to determine the impact that changes (e.g. reductions from abatement strategies) in emissions have on ambient air quality. Examples of this type of application include Federal rules and State Implementation Plans (SIPs) which aim to reduce emissions (through regulations) in order to meet mandated air quality standards. In this type of application, the air quality model is run using both baseline (often current year) and future year emissions (when emissions are typically lower due to state and national regulatory efforts) and then the change in criteria pollutant (e.g. O_3 and $PM_{2.5}$) concentrations between the two simulations is quantified in order to assess the impact (benefit) that emission reductions will have on future ambient air quality. As such, it is important to establish the ability of the model to accurately simulate the future ambient air quality given a known change in emissions, which here is referred to as the model responsiveness (to emission changes).

Some previous analyses comparing observed changes in ambient air quality (over periods witnessing large reductions in emissions) to CMAQ estimated changes in ambient air quality (with estimated reductions in emissions) during the same period have shown that the model tends to underestimate the observed change in ambient O_3, suggesting the model may be under-responsive to the emission reductions impacting O_3 (Gilliland et al., 2008; Foley et al., 2015). The over/under responsiveness of the model to emission projections can have implications in the planning process for determining the extent to which emissions must be reduced in order to meet future air quality standards. In the following sections, we examine the model responsiveness to emission reductions in CMAQ v5.0.2 and v5.1 by computing the ratio of maximum daily 8-hr average (MDA8) O_3 mixing ratios and total $PM_{2.5}$ (and select $PM_{2.5}$ component species) between simulations using the base emissions inventories and those employing 50% reductions in NO_X,VOC and SO_X emissions in order to estimate a model responsiveness to the emission reductions for each version of the model. The model responsiveness for v5.1 is then compared to that of v5.0.2 to determine whether the model responsiveness increased, decreased or was unchanged in the new version of the model.

6.1 O_3

Figure 17 shows the difference in the ratio (emission cut simulation / base simulation) of MDA8 O_3 for the 50% cut in anthropogenic NO_X and VOC scenarios, binned by model MDA8 O_3 mixing ratio. Values greater than zero indicate v5.1 is more responsive to the NO_X or VOC cut than v5.0.2, while values less than zero indicate v5.1 is less responsive than v5.0.2. For both January and July, the median difference in ratio values for all bins for the 50% NO_X cut scenario are greater than zero, indicating that v5.1 is more responsive than v5.0.2 to the cut in NO_X. For the 50% cut in VOC emissions the difference in the ratio values is mixed across the two months and the different bins. For January, all of the bins indicate that v5.0.2 is more responsive than v5.1

to the 50% VOC cut, with the greatest difference occurring for MDA8 O_3 mixing ratios greater than 65 ppbV. For July, v5.1 is slightly more responsive to the VOC cut for MDA8 O_3 mixing ratios less than 75 ppbV and less responsive for MDA8 O_3 mixing ratios greater than 85 ppbV.

6.2 $PM_{2.5}$

Figure 18 shows the difference in the ratio (emission cut simulation / base simulation) of $PM_{2.5}$ and select $PM_{2.5}$ component species between v5.0.2 and v5.1 for January and July for a 50% cut in anthropogenic emissions of NO_X, VOC and SO_X. For January, the overall response of modeled $PM_{2.5}$ (PMIJ) to a 50% reduction in NO_X is primarily driven by a decrease in nitrate and its associated ammonium. CMAQ v5.1 $PM_{2.5}$ is slightly less responsive to NO_X reductions compared to v5.0.2, but is still overall quite similar. The VOC cut shows greater response with v5.1 than v5.0.2 in January in ANCOMIJ (non-carbon organic matter attached to primary organic carbon; Simon and Bhave, 2012), AUNSPECIJ (unspeciated PM), AOMIJ (all organic matter), AORGAJ (SOA from anthropogenic VOCs) and AORGBJ (SOA from biogenic VOCs) and total $PM_{2.5}$ (see S.2 and S.3). Note that the letters I and J after the species name indicate which CMAQ modal distributions are being included in the total species mass, with I indicating the Aitken mode and J indicating the Accumulation mode. Since NCOMIJ is nonvolatile, its change reflects how reducing VOCs changes oxidants such as OH. In general, the model $PM_{2.5}$ is not very sensitive to VOC cuts in January. And finally, for the 50% SO_X cut scenario $PM_{2.5}$ is only slightly less responsive with v5.1, with all the species being similarly responsive to the SO_X cut using v5.1 compared to v5.0.2.

For July, the NO_X cut scenario with v5.1 shows greater responsiveness for the ASO4IJ (sulfate), ANH4IJ (nitrate), AECIJ (elemental carbon), APOAIJ (primary organic aerosol), AORGCJ (SOA from glyoxal and methylglyoxal processing in clouds) species and total $PM_{2.5}$ versus v5.0.2. For the VOC cut scenario, the AORGAJ species show increased responsiveness with v5.1. CMAQv5.1 alkane SOA is not dependent on NO_X levels or HO_2:NO ratios, so the decrease in VOC precursors have a more direct effect than for the aromatic systems (the only AORGAJ in v5.0.2), where decreasing the VOC precursors can also modify the HO_2:NO ratio and thus yields. CMAQ v5.1 PMIJ becomes slightly more responsive to SO_X cut as a result of an increased sensitivity of biogenic SOA to sulfur containing compounds. This link results from the IEPOX acid-catalyzed SOA in the model which has been shown to be correlated with sulfate (Pye et al., 2016).

7 Summary

A new version of the CMAQ model (v5.1) containing numerous scientific updates has been released and evaluated in terms of the change in performance against the previous version of the model (v5.0.2), performance compared to observations, and response to changes in inputs (i.e. emissions). Specifically, updates were made to the ACM2 scheme in both WRF and CMAQ to improve the vertical mixing in both models, along with updates to the MOL calculation, which also directly impacted the vertical mixing in the WRF-CMAQ system. The overall net effect of these updates was to increase the ventilation in the model, particularly during the transition periods (morning and evening), which in turn reduced the concentration of primary emitted species (e.g. NO_X and OC) and consequently increased simulated O_3 (a result of reduced NO_X titration) and decreased $PM_{2.5}$ concentrations due to greater dilution. Several new SOA formation pathways and species were added to v5.1, resulting in increased SOA, particularly in the southeast U.S., and improved $PM_{2.5}$ performance in the summer, as $PM_{2.5}$ is generally underestimated by CMAQ during the summer in the U.S.

The in-line photolysis model within CMAQ was updated in v5.1. Cloud cover for the photolysis model in v5.0.2 used a single cloud deck with a constant cloud fraction and water droplet mixing ratio. In v5.1, multiple cloud decks with variable cloud fractions and multiple types of water condensates are used in the photolysis model to be more consistent with the WRF meteorological model and the CMAQ cloud model. The net effect of this change was to decrease the amount of sub-grid clouds in the photolysis calculation in v5.1, which in turn results in higher photolysis rates and thus higher predicted O_3 mixing ratios on average. In addition to the change to the photolysis model, the refractive indices for aerosol species are now both wavelength and composition dependent. Changes in aerosol scattering and extinction also introduce options for how to calculate their optical properties and allow the user to specify which aerosol mixing model and method to use to solve the Mie scattering theory. The atmospheric chemistry in the model has also been updated from CB05TUCL to CB05e51 in v5.1, which includes, among other things, updates to the NO_Y reactions, additional isoprene extensions, explicit representation of several HAPs, and a simple parameterization of the effects of halogens on O_3 in marine environments. The net effect of going from CB05TUCL to CB05e51 was to increase O_3 in the winter and summer, while increasing $PM_{2.5}$ slightly in the winter and increasing/decreasing $PM_{2.5}$ slightly in the summer.

Overall, the scientific updates in v5.1 resulted in relatively dramatic improvements in model performance for $PM_{2.5}$ in the winter and summer and small overall changes in performance during spring and fall. $PM_{2.5}$ concentrations decreased significantly in v5.1 in the winter when $PM_{2.5}$ is typically overestimated by CMAQ over the U.S., and increased significantly in the summer when $PM_{2.5}$ is typically underestimated by the model. The change in O_3 mixing ratios in v5.1 resulted in mixed improvement in MB, both spatially and temporally, with the summer showing the largest increase in MB. However, RMSE largely improved regardless of season and showed a larger improvement spatially across the sites than MB, and the correlation is almost always higher with v5.1. Comparisons of vertical profiles of several species taken over Edgewood, MD during the DISCOVER-AQ campaign showed improved performance with v5.1 throughout the PBL for O_3, NO_2, NO_Y, ANs and CO, with the PNs being the only species to show degraded performance on that day.

The response of the model to changes in emission inputs was examined by comparing the ratio of the base v5.0.2 and v5.1 simulations to sensitivity simulations with 50% cuts each to anthropogenic NO_X, VOC and SO_X emissions. CMAQv5.1 simulated MDA8 O_3 exhibited more responsiveness (greater reduction) to the 50% NO_X cut in January and July than v5.0.2, which is considered an improvement as previous studies suggested CMAQ O_3 to be under-responsive to large changes in emissions. The responsiveness of $PM_{2.5}$ to the emission cuts is more complicated than for O_3 since there are many more species comprising $PM_{2.5}$ and some of those have greater or smaller response with v5.1. However, the new pathways of formation for several $PM_{2.5}$ components in v5.1 generally result

+3+ in greater responsiveness in v5.1 compared to v5.0.2 for the various emission cut scenarios.

Finally, a number of important science updates are in development and will be available in the next release of CMAQ (v5.2), which improve upon the existing science in the model. These updates include a new version of the windblown dust treatment (Foroutan et al., 2016), the Carbon-Bond 6 (CB6) chemical mechanism (Ramboll Environ, 2016), enhancements to the calculation of semi-volatile Primary Organic Aerosol (POA) and SOA from combustion sources in CMAQ (Pye et al., 2016), and additional updates to the calculation of clouds. In addition to the model updates, a number of instrumented versions of the model (e.g. decoupled direct method, sulfur tracking) will also be released with v5.2. These updates represent potentially significant improvements over the current options in v5.1 (specifically the updated windblown dust treatment) and therefore are being made available to the community more quickly than they might have in the past.

Code availability

CMAQ model documentation and released versions of the source code, including all model code used in this study, are available at www.cmaq-model.org. The updates described here, as well as model post-processing scripts, are available upon request. The WRF model is available for download through the WRF website (http://www.wrf-model.org/index.php).

Data availability

The raw observation data used are available from the sources identified in Section 3, while the post-processed observation data are available upon request. The CMAQ model data utilized are available upon request as well.

Disclaimer

The views expressed in this article are those of the authors and do not necessarily represent the views or policies of the U.S. Environmental Protection Agency.

Acknowledgements

The authors would like to think CSRA for creating the WRF meteorological inputs and emissions data used in the various model simulations. The authors would also like to thank the DISCOVER-AQ project (DOI: 10.5067/Aircraft/DISCOVER-AQ/Aerosol-TraceGas) for providing some of the data used in this work.

References

Altimir, N., Kolari, P., Tuovinen, J.-P., Vesala, T., Bäck, J., Suni, T., Kulmala, M., and Hari, P.: Foliage surface ozone deposition: a role for surface moisture?, Biogeosciences, 3, 209-228, doi:10.5194/bg-3-209-2006, 2006.

Anderson, D. C., Loughner, C. P., Diskin, G., Weinheimer, A., Canty, T. P., Salwitch, R. J., Worden, H. M., Fried, A., Mikoviny, T., Wisthaler, A., and Dickerson, R. R.: Measured and modeled CO and NO_Y in DISCOVER-AQ: An evaluation of emissions and chemistry over the eastern US, Atmos. Environ., 96, 78-87, doi:10.1016/j.atmosenv.2014.07004, 2014.

Appel, K. W., Bhave, P. V., Gilliland, A. B., Sarwar, G., and Roselle, S. J.: Evaluation of the Community Multiscale Air Quality (CMAQ) model version 4.5: Sensitivities impacting model performance; Part II - particulate matter, Atmos. Environ., 42(24), 6057-6066, doi:10.1016/j.atmosenv.2008.03.036, 2008.

Appel, K.W., Chemel, C., Roselle, S.J., Francis, X.V., Sokhi, R.S., Rao, S.T., and Galmarini, S.: Examination of the Community Multiscale Air Quality (CMAQ) model performance over the North American and European Domains, Atmos. Environ., doi:10.1016/j.atmosenv.2011.11.016, 53, 142-155, 2012.

Appel, K. W., Gilliland, A. B., Sarwar, G., and Gilliam, R. C.: Evaluation of the Community Multiscale Air Quality (CMAQ) model version 4.5: Sensitivities impacting model performance; Part I – ozone, Atmos. Environ., 41(40), 9603-9615, doi:10.1016/j.atmosenvv.2007.08.044, 2007.

Appel, K. W., Gilliam, R. C., Davis, N., Zubrow, A., and Howard, S. C.: Overview of the Atmospheric Model Evaluation Tool (AMET) v1.1 for evaluating meteorological and air quality models, Environ. Modell. Softw., 26, 4, 434-443, 2011.

Appel, K. W., Pouliot, G. A., Simon, H., Sarwar, G., Pye, H. O. T., Napelenok, S. L., Akhtar, F., and Roselle, S. J.: Evaluation of dust and trace metal estimates from the Community Multiscale Air Quality (CMAQ) model version 5.0, Geosci. Model Dev., 6, 883-899, doi:10.5194/gmd-6-883-2013, 2013.

Bash, J.O., Baker, K.R., and Beaver, M.R.: Evalution of improved land use and canopy representation in BEIS v3.61 with biogenic VOC measurements in California, Geosci. Model Dev., 9, 2191-2207, doi:10.5194/gmd-9-2191-2016, 2016.

Bond, T. C. and Bergstrom, R. W.: Light absorption by carbonaceous particles: An investigative review, Aero. Sci. Tech., 40(1), 27-67, doi:10.1080/02786820500421521, 2006.

Bey, I., Jacob, D. J., Yantosca, R. M., Logan, J. A., Field, B. D., Fiore, A. M., Li, Q., Liu, H. Y., Mickley, L. J., and Schultz, M. G.: Global modeling of tropospheric chemistry with assimilated meteorology: Model description and evaluation, J. of Geophys. Res., 106, 23073-23096, 2001.

Bridier, I., Caralp, F., Loirat, H., Lesclaux, R., Veyret, B., Becker, K. H., Reimer, A., and Zabel, F.: Kinetic and theoretical studies of the reactions acetylperoxy + nitrogen dioxide + M .dblarw. acetyl peroxynitrate + M between 248 and 393 K and between 30 and 760 torr, J. Phys. Chem., 95, 3594-3600, 1991.

Butkovskaya, N., Kukui, A., and Le Bras, G.: HNO_3 forming channel of the HO2+NO reaction as a function of pressure and temperature in the ranges of 72-600 Torr and 223-323 K, J. Phys. Chem. A, 111(37), 9047-9053, 2007.

Byun, D. and Schere, K. L.: Review of the governing equations, computational algorithms, and other components of the Models-3 Community Multiscale Air Quality (CMAQ) modeling system, Appl. Mech. Rev., 59, 51-77, 2006.

Carlton, A. G., Bhave, P. V., Napelenok, S. L., Edney, E. D., Sarwar, G., Pinder, R. W., Pouliot, G. A., and Houyoux, M.: Model representation of secondary organic aerosol in CMAQv4.7, Environ. Sci. Technol., 44 (22), 8553-8560, 2010.

Chang, H. and Charalampopoulos, T. T.: Determination of the wavelength dependence of reactive indices on flame soot, Proc. R. Soc. Lond. A 1990 430, 577-591, doi:10.1098/rspa.1990.0107, 1990.

de Leeuw, G., Andreas, E.L., Anguelova, M.D., Fairall, C.W., Lewis, E.R., O'Dowd, C., Schulz, M., Schwartz, S.W.: Production flux of sea spray aerosol, Rev. Geophys., 49, RG2001, doi:10.1029/2010RG000349, 2011.

Echer, F.R. and Rosolem, C.A.: Cotton leaf gas exchange responses to irradiance and leaf aging. Biologia Plantarum, 59(2), pp.366-372, 2015.

Eder, B., Kang, D., Mathur, R., Yu, S., Schere, K.: An Operational evaluation of the Eta-CMAQ air quality forecast model, Atmos. Environ. 40, 4894 – 4905, 2006.

Fann, N., Fulcher, C.M., and Hubbell, B.J.: The influence of location, source, and emission type in estimates of the human health benefits of reducing a ton of air pollution, Air Qual. Atmos. Health, 2, 169-176, 2009.

Foley, K. M., Hogrefe, C., Pouliot, G., Possiel, N., Roselle, S. J., Simon, H., and Timin, B.: Dynamic evaluation of CMAQ part I: Separating the effects of changing emissions and changing meteorology on ozone levels between 2002 and 2005 in the eastern U.S., Atmos. Environ., 103, 247-255, doi:10.1016/j.atmosenv.2014.12.038, 2015.

Foley, K.M., Roselle, S.J., Appel, K.W., Bhave, P.V., Pleim, J.E., Otte, T.L., Mathur, R., Sarwar, G., Young, J.O., Gilliam, R.C., Nolte, C.G., Kelly, J.T., Gilliland, A.B., and Bash, J.O.: Incremental testing of the Community Multiscale Air Quality (CMAQ) modeling system version 4.7, Geosci. Model Dev., 3, 205-226, doi:10.5194/gmd-3-205-2010, 2010.

Foroutan, H., Young, J., Napelenok, S., Ran, L., Appel, K. W., and Pleim, J. E.: Development and evaluation of a physics-based windblown dust emission scheme in the CMAQ modeling system, J. Geophys. Res., 2016.

Gantt, B., Kelly, J. T., and Bash, J. O.: Updating sea spray aerosol emission in the Community Multiscale Air Quality (CMAQ) model version 5.0.2, Geosci. Model Dev., 8, 3733-3746, doi:10.5194/gmd-8-3733-2015, 2015.

Gilliland, A. B., Hogrefe, C., Pinder, R. W., Godowitch, J. M., Foley, K. M., and Rao, S. T.: Dynamic evaluation of regional air quality models: Assessing changes in O_3 stemming from changes in emissions and meteorology, Atmos. Environ., 42(20), 5110-5123, doi:10.1016/j.atmosenv.2008.02.018, 2008.

Giard, D. and Bazile, E.: Implementation of a new assimilation scheme for soil and surface variables in a global NWP model. Mon. Wea. Rev., 128, 997-1015, 2000.

Gong, S.L.: A parameterization of sea-salt aerosol source function for sub- and super-micron particles, Global Biogeochem. Cy., 17, 1097, doi:10.1029/2003gb002079, 2003.

Guenther, A., Karl, T., Harley, P., Wiedinmyer, C., Plamer, P. I., and Geron, C.: Estimates of global terrestrial isoprene emissions using MEGAN (Model of emissions of Gases and Aerosols from Nature), Atmos. Chem. Phys., 6, 3181-3210, 2006.

Hess, M., Koepke, P., and Schult, I.: Optical properties of aerosols and clouds: The software package OPAC, B. Am. Meteorol. Soc., 79(5), 831-844, 1998.

Hildebrandt Ruiz, L. and Yarwood, G.: Interactions between Organic Aerosol and NO_Y: Influence on Oxidant Production, Final report for AQRP project 12-012, http://aqrp.ceer.utexas.edu/projectinfoFY12_13/12-012/12-012%20Final%20Report.pdf, 2013.

Hu, W. W., Campuzano-Jost, P., Palm, B. B., Day, D. A., Ortega, A. M., Hayes, P. L., Krechmer, J. E., Chen, Q., Kuwata, M., Liu, Y. J., de Sá, S. S., McKinney, K., Martin, S. T., Hu, M., Budisulistiorini, S. H., Riva, M., Surratt, J. D., St. Clair, J. M., Isaacman-Van Wertz, G., Yee, L. D., Goldstein, A. H., Carbone, S., Brito, J., Artaxo, P., de Gouw, J. A., Koss, A., Wisthaler, A., Mikoviny, T., Karl, T., Kaser, L., Jud, W., Hansel, A., Docherty, K. S., Alexander, M. L., Robinson, N. H., Coe, H., Allan, J. D., Canagaratna, M. R., Paulot, F., and Jimenez, J. L.: Characterization of a real-time tracer for isoprene epoxydiols-derived secondary organic aerosol (IEPOX-SOA) from aerosol mass spectrometer measurements, Atmos. Chem. Phys., 15, 11807-11833, doi:10.5194/acp-15-11807-2015, 2015.

Iacono M.J., Delamere, J. S., Mlawer, E. J., Shephard, M. W., Clough, S. A., and Collins, W.: Radiative forcing by long-lived greenhouse gases: Calculations with the AER radiative transfer models, J. Geophys. Res., 113, D13103, doi:10.1029/2008JD009944, 2008.

Jaeglé, L., Quinn, P. K., Bates, T. S., Alexander, B., and Lin, J.-T.: Global distribution of sea salt aerosols: new constraints from in situ and remote sensing observations, Atmos. Chem. Phys., 11, 3131-2157, doi:10.5194/acp-11-3137-2011, 2011.

Jathar, S. H., T. D. Gordon, C. J. Hennigan, H. O. T. Pye, G. Pouliot, P. J. Adams, N. M. Donahue, and A. L. Robinson, Unspeciated organic emissions from combustion sources and their influence on the secondary organic aerosol budget in the United States, Proc. Natl. Acad. Sci. USA, 2014.

Jayalakshmy, M. S. and Philip, J.: Thermophysical properties of plant leaves and their influence on the environment temperature, Int. J. Thermophys., 31:2295, doi:10.1007/s10765-010-0877-7, 2010.

Jenkin, M.E., Young, J.C., Rickard, A.R.: The MCM v3.3 degradation scheme for isoprene. Atmos. Chem. Phys. Discuss., 15, 9709-9766, 2015.

Kain, J. S.: The Kain-Fritsch convective parameterization: An update, J. Appl. Meteor., 43, 170-181, 2004.

Lee, L., Teng, A. P., Wennberg, P. O., Crounse, J. D., and Cohen, R. C.: On Rates and Mechanisms of OH and O_3 Reactions with Isoprene-Derived Hydroxy Nitrates, J. Phys. Chem. A, 118, 1622-1637, 2014.

Liu, S., Shilling, J. E., Song, C., Hiranuma, N., Zaveri, R. A., and Russell, L. M.: Hydrolysis of Organonitrate Functional Groups in Aerosol Particles, Aerosol Sci. Technol., 46, 1359-1369, 2012.

Marais, E. A., Jacob, D. J., Jimenez, J. L., Campuzano-Jost, P., Day, D. A., Hu, W., Krechmer, J., Zhu, L., Kim, P. S., Miller, C. C., Fisher, J. A., Travis, K., Yu, K., Hanisco, T. F., Wolfe, G. M., Arkinson, H. L., Pye, H. O. T., Froyd, K. D., Liao, J., and

McNeill, V. F.: Aqueous-phase mechanism for secondary organic aerosol formation from isoprene: application to the southeast United States and co-benefit of SO_2 emission controls, Atmos. Chem. Phys., 16, 1603-1618, doi:10.5194/acp-16-1603-2016, 2016.

McNeill, V. F., Woo, J. L., Kim, D. D., Schwier, A. N., Wannell, N. J., Sumner, A. J., and Barakat, J. M.: Aqueous-phase Secondary Organic Aerosol and Organosulfate Formation in Atmospheric Aerosols: A Modeling Study, Environ. Sci. Technol., 46 (15), 8075–8081, 2012.

Mebust, M. R., Eder, B. K., Binkowski, F. S., and Roselle, S. J.: Models-3 Community Multiscale Air Quality (CMAQ) model aerosol component, J. Geophys. Res., 108(D6), 4184, doi:10.1029/2001JD001410, 2003.

Mocko, D.M. and Cotton, W.R.: Evaluation of fractional cloudiness parameterizations for use in a mesoscale model, J. Atmos. Sci., 52(16), 2884-2901, 1995.

Morrison, H., Curry, J. A., and Khvorostyanov, V. I.: A new doublemoment microphysics parameterization for application in cloud and climate models. Part I: Description, J. Atmos. Sci., 62, 1665–1677, 2005.

Nenes, A., Pandis, S. N., and Pilinis, C.: ISORROPIA: A new thermodynamic equilibrium model for multiphase multicomponent inorganic aerosols, Aquat. Geochem., 4(1), 123-152, 1998.

Nenes, A., Pandis, S. N., and Pilinis, C.: Continued development and testing of a new thermodynamic aerosol module for urban and regional air quality models, Atmos. Environ., 33(10), 1553-1560, 1999.

Niinemets, Ü., Arneth, A., Kuhn, U., Monson, R. K., Peñuelas, J., and Staudt, M.: The emission factor of volatile isoprenoids: stress, acclimation, and developmental responses, Biogeosciences, 7, 2203–2223, doi:10.5194/bg-7-2203-2010, 2010.

Nolte, C. G., Appel, K. W., Kelly, J. T., Bhave, P. V., Fahey, K. M., Collett Jr., J. L., Zhang, L., and Young, J. O.: Evaluation of the Community Multiscale Air Quality (CMAQ) model v5.0 against size-resolved measurements of inorganic particle composition across sites in North America, Geosci. Model Dev., 8, 2877-2892, doi:10.5194/gmd-8-2877-2015, 2015.

Nolte, C. G., Gilliland, A. B., Hogrefe, C., and Mickley, L. J.: Linking global to regional models to assess future climate impacts on surface ozone levels in the United States, J. Geophys. Res., 113, D14307, doi:10.1029/2007JD008497, 2008.

Otte, T. L. and Pleim, J. E.: The Meteorology-Chemistry Interface Processor (MCIP) for the CMAQ modeling system: updates through MCIPv3.4.1, Geosci. Model Dev., 3, 243-256, doi:10.5194/gmd-3-243-2010, 2010.

Ovadnevaite, J., Manders, A., de Leeuw, G., Ceburnis, D., Monahan, C., Partanen, A.-I., Korhonen, H., and O'Dowd, C. D.: A sea spray flux parameterization encapsulating wave state, Atmos. Chem. Phys., 14, 1837-1852, doi:10.5194/acp-14/1837-2014, 2014.

Pleim, J. E.: A combined local and nonlocal closure model for the atmospheric boundary layer. Part I: model description and testing, J. Appl. Meteor. Clim., 46, 1383-1395, 2007a.

Pleim, J. E.: A combined local and nonlocal closure model for the atmospheric boundary layer. Part II: application and evaluation in a mesoscale meteorological model, J. Appl. Meteor. Clim., 46, 1396–1409, 2007b.

Pleim J. E. and Gilliam, R. C.: An indirect data assimilation scheme for deep soil temperature in the Pleim-Xiu land surface model, J. Appl. Meteor. Clim., 48, 1362-1376, 2009.

Pleim, J. E., Gilliam, R. C., Appel, K. W., and Ran. L.: Recent advances in modeling of the atmospheric boundary layer and land-surface in the coupled WRF-CMAQ model, 34th International Technical Meeting on Air Pollution and its Application, 4-8 May, Montpellier, France, 2015.

Pleim, J., Roselle, S., Young, J., Schwede, D., Mathur, R., and Bhave, P.: New Developments in CMAQ Model Physics, Presented at 4th Annual CMAS Models-3 Users' Conference.

September 26-28, 2005, UNC-Chapel Hill https://www.cmascenter.org/conference/2005/ppt/1_1.pdf, 2005.

Pleim, J. E. and Xiu, A.: Development and testing of a surface flux and planetary boundary layer model for application in mesoscale models, J. Appl. Meteor., 34, 16–32, 1995.

Pye, H. O. T., Luecken D. J., Xu, L., Boyd, C. M., Ng, N. L., Baker, K., Ayres, B. A., Bash, J. O., Baumann, K., Carter, W. P. L., Edgerton, E., Fry, J. L., Hutzell, W. T., Schwede, D., and Shepson, P. B.: Modeling the current and future roles of particulate organic nitrates in the southeastern United States, Environ. Sci. Technol., 49, 14195-14203, doi:10.1021/acs.est.5b03738, 2015.

Pye, H. O. T., Murphy, B. N., Xu, L., Ng, N. L., Carlton, A. G., Guo, H., Weber, R., Vasilakos, P., Appel, K. W., Budisulistiorini, S. H., Surratt, J. D., Nenes, A., Hu, W., Jimenez, J. L., Isaacman-VanWertz, G., Misztal, P. K., and Goldstein, A. H.: On the implications of aerosol liquid water and phase separation for organic aerosol mass, Atmos. Chem. Phys. Discuss., doi:10.5194/acp-2016-719, in review, 2016.

Pye, H. O. T., Pinder, R. W., Piletic, I., Xie, Y., Capps, S. L., Lin, Y.-H., Surratt, J. D., Zhang, Z., Gold, A., Luecken, D. J., Hutzell, W. T., Jaoui, M., Offenberg, J. H., Kleindienst, T. E., Lewandowski, M., and Edney, E. O.: Epoxide pathways improve model predictions of isoprene markers and reveal key role of acidity in aerosol formation, Environ. Sci. Technol., 47 (19), 11056-11064, 2013.

Pye, H. O. T. and Pouliot, G. A.: Modeling the role of alkanes, polycyclic aromatic hydrocarbons, and their oligomers in secondary organic aerosol formation, Environ. Sci. Technol., 46 (11), 6041-6047, 2012.

Ramboll Environ.: User's Guide Comprehensive Air Quality Model with Extensions, version 6.3, Novato, CA, http://www.camx.com/files/camxusersguide_v6-30.pdf, 2016.

Rollins, A. W., Pusede, S., Wooldridge, P., Min, K .E., Gentner, D. R., Goldstein, A. H., Liu, S., Day, D. A., Russell, L .M., Rubitschun, C. L., Surratt, J. D., and Cohen, R. C.: Gas/particle partitioning of total alkyl nitrates observed with TD-LIF in Bakersfield. J. Geophys. Res. Atmos., 118, 6651-6662, 2013.

Sarwar, G., Simon, H., Bhave, P. V., Yarwood, G.: Examining the impact of heterogeneous nitry chloride production on air quality across the United States, Atmos. Phys. Chem., 12, 6455-6473, 2012.

Scheffe, R., Hubbell, B., Fox, T., Rao, V., and Pennell, W.: The rationale for a multipollutant, multimedia air quality management framework, EM Magazine, 14-20, May 2007.

Segelstein, D.: The complex refractive index of water, M.S. Thesis, University of Missouri—Kansas City, MO, 1981.

Simon, H. and Bhave, P. V.: Simulating the degree of oxidation in atmospheric organic particles, Environ. Sci. Technol., 46(1), 331-339, doi:10.1021/es202361w, 2012.

Simon, H., Beck, L., Bhave, P., Divita, F., Hsu, Y., Luecken, D., Mobley, D., Pouliot, G., Reff, A., Sarwar, G., and Strum, M.: The development and uses of EPA's SPECIATE database, Atmos. Pollut. Res., 1, 196-206, 2010.

Skamarock, W. C., Klemp, J. B., Dudhia, J., Gill, D. O., Barker, D. M., Duda, M. G., Huang, X-Y, Wang, W., and Powers, J. G.: A description of the advanced research WRF version 3. NCAR Tech Note NCAR/TN 475 STR, 125 pp, [Available from UCAR Communications, P.O. Box 3000, Boulder, CO 80307.], 2008.

Sundqvist, H., Berge, E., and Kristjánsson, J.E.: Condensation and cloud parameterization studies with mesoscale numerical weather prediction model, Mon. Wea. Rev., 117, 1641-1657, 1989.

Surratt, J. D., Chan, A. W. H., Eddingsaas, N. C., Chan, M. N., Loza, C. L., Kwan, A. J., Hersey, S. P., Flagan, R. C., Wennberg, P. O., and Seinfeld, J. H.: Reactive intermediates revealed in secondary organic aerosol formation from isoprene, P. Natl. Acad. Sci. USA, 107(15), 6640-6645, doi:10.1073/pnas.0911114107, 2010.

Swall, J. and Foley, K. M.: The impact of spatial correlation and incommensurability on model evaluation, Atmos. Environ., 43(6), 1204-1217, 2009.

Toon, O. B., McKay, C. P., Ackerman, T. P., and Santhanam, K.: Rapid calculation of radiative heating rates and photodissociation rates in inhomogeneous multiple scattering atmospheres: J. Geophys. Res. 94, 16287-16301, 1989.

Troe, J.: Refined Representation of Falloff Curves for the Reaction HO + NO2 + N2 → (HONO2, HOONO) + N2, J. Phys. Chem. A, 116, 6387-6393, 2012.

Wesely, M.L.: Parameterization of surface resistances to gaseous dry deposition in regional scale models, Atmos. Environ., 23(6), 1293-1304, 1989.

Whitten, G.Z., Heo, G., Kimura, Y., McDonald-Buller, E., Allen, D.T., Carter, W.P.L., and Yarwood, G.: A new condensed toluene mechanism for Carbon Bond: CB05-TU, Atmos. Environ., 44, 5346-5355, 2010.

Wild, O., Zhu, X., and Prather, M. J.: Fast-J: Accurate simulation of in- and below-cloud photolysis in tropospheric chemical models, J. Atmos. Chem., 37(3), 245-282, doi:10.1023/A:1006415919030, 2000.

Woody, M. C., Baker, K. R., Hayes, P. L., Jimenez, J. L., Koo, B., and Pye, H. O. T.: Understanding sources of organic aerosol during CalNex-2010 using the CMAQ-VBS, Atmos. Chem. Phys., 16, 4081-4100, doi:10.5194/acp-16-4081-2016, 2016.

Table 1: New/revised SOA species in the CMAQ v5.1 AERO6 mechanism.

Aerosol Species	Change since v5.0.2	Applicable Mechanism	Description of Modification
AH3OP	added	all	Hydronium ion (predicted by ISORROPIA for I+J modes), used for IEPOX uptake
APAH1,2	added	cb05e51, saprc07tb, saprc07tc, saprc07tic, racm	Naphthalene aerosol from RO_2+NO reactions
APAH3	added	cb05e51, saprc07tb, saprc07tc, saprc07tic, racm	Naphthalene aerosol from RO_2+HO_2 reactions
AISO1,2	updated	cb05e51, saprc07tb, saprc07tc*, racm	Aerosol from isoprene reactions NO_3 added to existing OH (all yields follow the OH pathway)
AISO3	updated	cb05e51, saprc07tb, saprc07tc*, racm	Aerosol from reactive uptake of IEPOX on aqueous aerosol particles. Specifically intended to be the sum of 2-methyltetrols and IEPOX-derived organosulfates.
AALK1,2	added	cb05e51, saprc07tb, saprc07tc, saprc07tic, racm	Alkane aerosol
AALK	removed	all	deprecated alkane aerosol

*AERO6i does not include SOA from isoprene+NO3 in AISO1,2 (it is included in AISOPNNJ). AERO6i does not include IEPOX SOA in AISO3 (it is included in AITETJ, AIEOSJ, AIDIMJ, etc). AISO3 is approximately zero in AERO6i.

Table 2: Description of the CMAQ model simulations utilized.

CMAQ Simulation Name	CMAQ version	WRF Version	NEI Version	Photolysis Scheme	Chemical Mechanism	Simulation Period
CMAQv5.0.2_Base	v5.0.2	v3.4	v1	v5.0.2	CB05TUCL	Annual (2011)
CMAQv5.0.2_WRFv3.7	v5.0.2	v3.7	v1	v5.0.2	CB05TUCL	January and July 2011
CMAQv5.1_Base	v5.1	v3.7	v2	v5.1	CB05e51	Annual (2011)
CMAQv5.1_RetroPhot	v5.1	v3.7	v2	v5.0.2	CB05e51	January and July 2011
CMAQv5.1_TUCL	v5.1	v3.7	v2	v5.1	CB05TUCL	January and July 2011

a) January O_3 diff (CMAQv5.0.2_WRFv3.7 – CMAQv5.0.2_Base)

b) July O_3 diff (CMAQv5.0.2_WRFv3.7 – CMAQv5.0.2_Base)

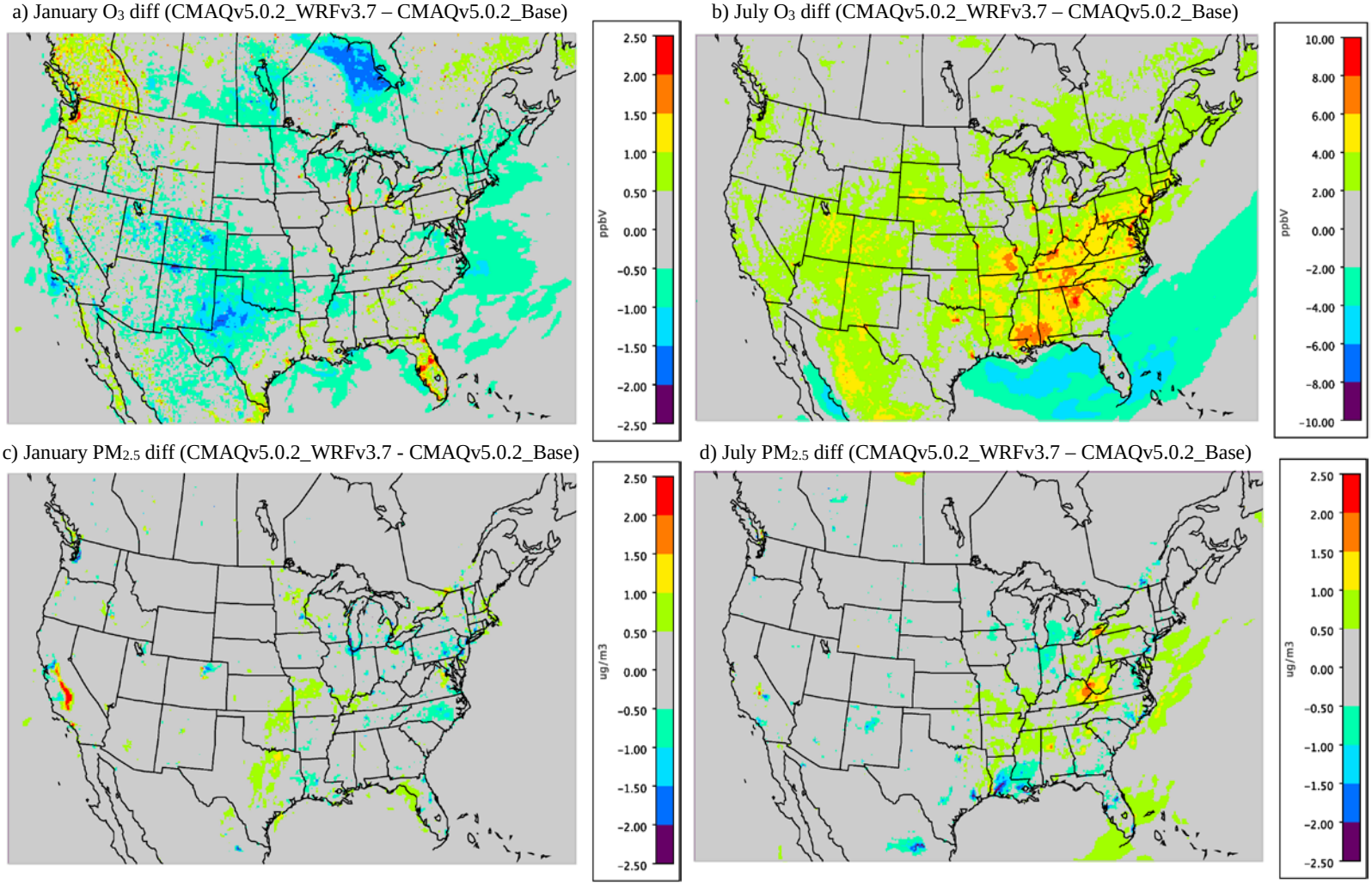

c) January $PM_{2.5}$ diff (CMAQv5.0.2_WRFv3.7 - CMAQv5.0.2_Base)

d) July $PM_{2.5}$ diff (CMAQv5.0.2_WRFv3.7 – CMAQv5.0.2_Base)

Figure 1: Monthly average difference in O_3 (ppbv) for a) January and b) July and $PM_{2.5}$ (μgm^{-3}) for c) January and d) July between CMAQv5.0.2 using WRFv3.4 (CMAQv5.0.2_Base) and CMAQv5.0.2 using WRFv3.7 (CMAQv5.0.2_WRFv3.7) (CMAQv5.0.2_WRFv3.7 – CMAQv5.0.2_Base). Note that the scales for each plot can vary.

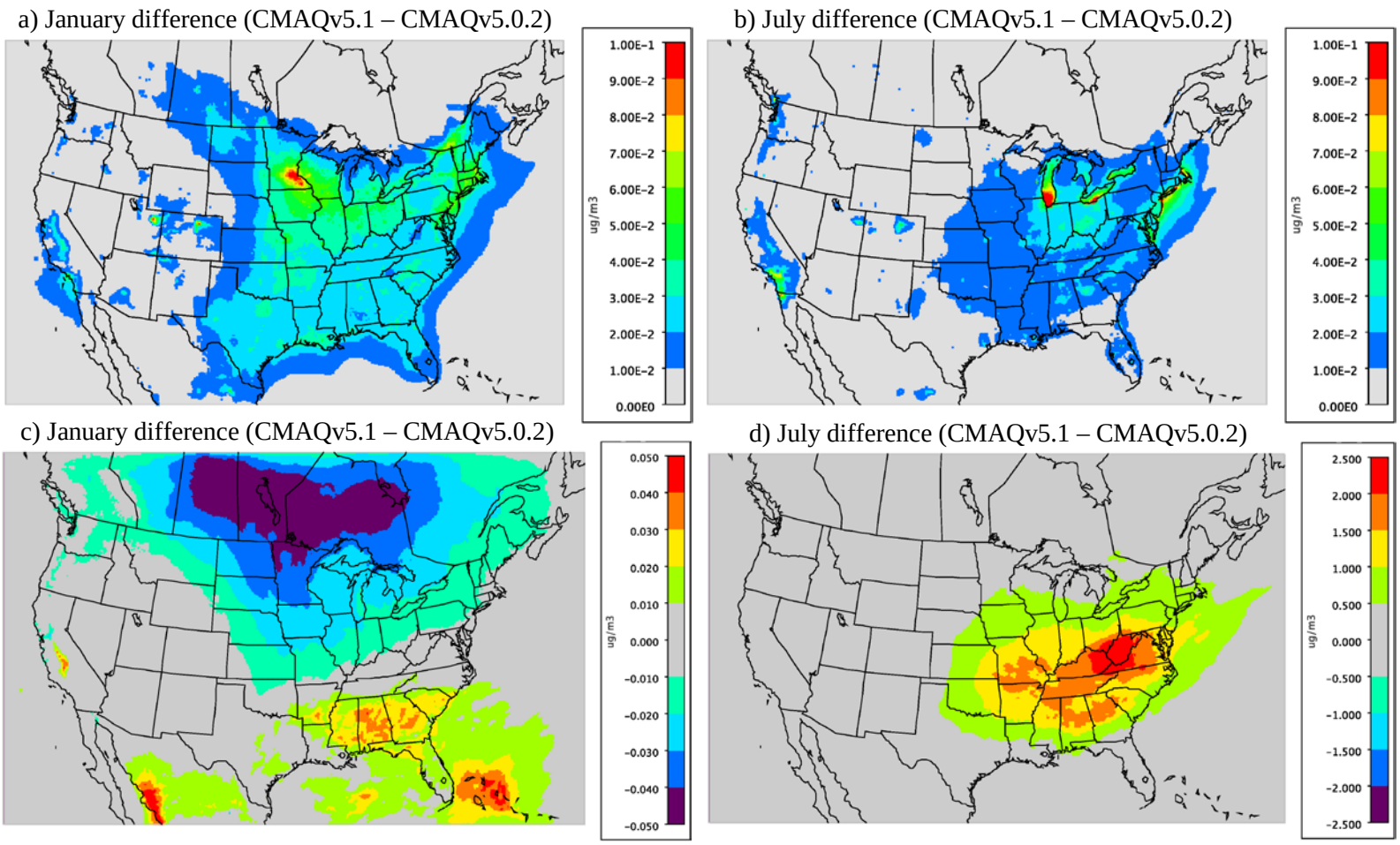

Figure 2: Monthly average sum total of AALK1, AALK2, APAH1, APAH2 and APAH3 for a) January and b) July (upper right) and the monthly average difference is the sum total of AISO1, AISO2, AISO3 and AOLGB for c) January and d) July between the aerosol treatments in CMAQ v5.0.2 and v5.1 (v5.1 – v5.0.2). All plots are in units of µgm^{-3}. Note that the scales for each plot can vary.

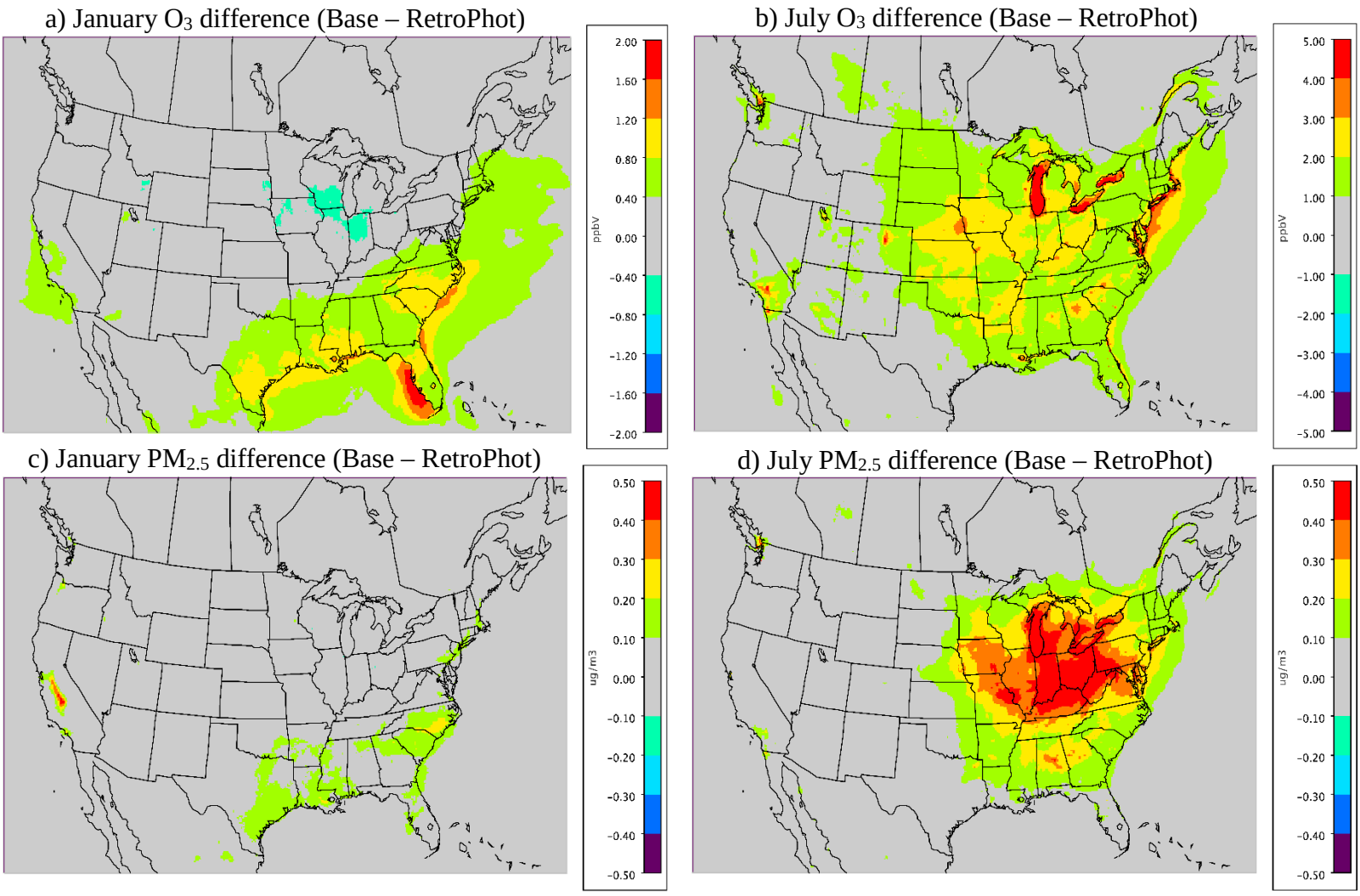

Figure 3: Difference in the monthly average O_3 for a) January and b) July and $PM_{2.5}$ for c) January and d) July between CMAQ v5.1_base and v5.1_RetroPhot (v5.1_Base – v5.1_RetroPhot). O_3 plots are in units of ppb and $PM_{2.5}$ plots are in units of µgm^{-3}. Note that the scales for each plot can vary.

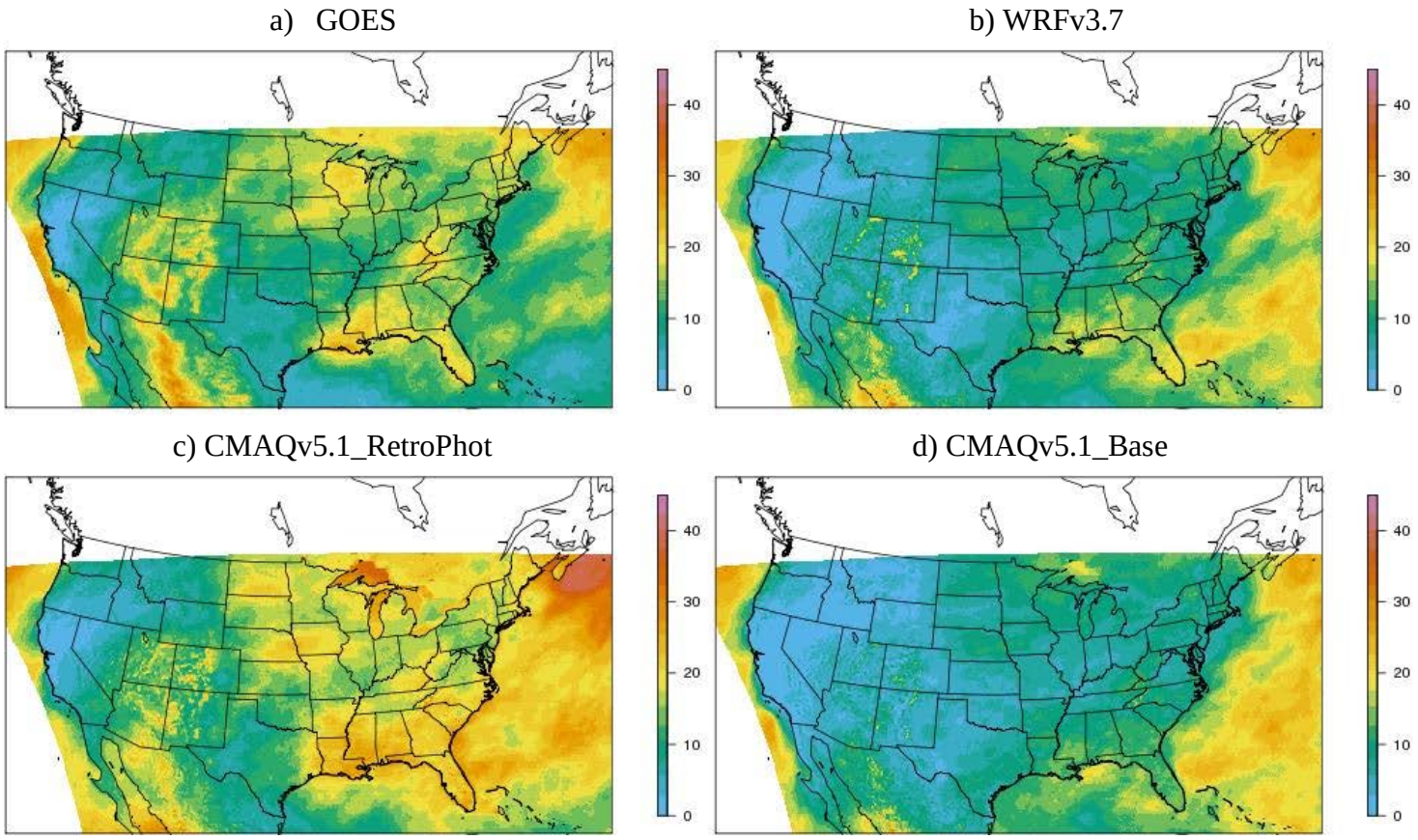

Figure 4. The average cloud albedo during daytime hours in July 2011 derived from (a) the GOES satellite product (b) WRF3.7 (c) CMAQv5.1 with photolysis/cloud model treatment from v5.0.2 and WRF3.7 inputs (CMAQv5.1_RetroPhot) (d) CMAQv5.1 using WRF3.7 inputs (CMAQv5.1_Base).

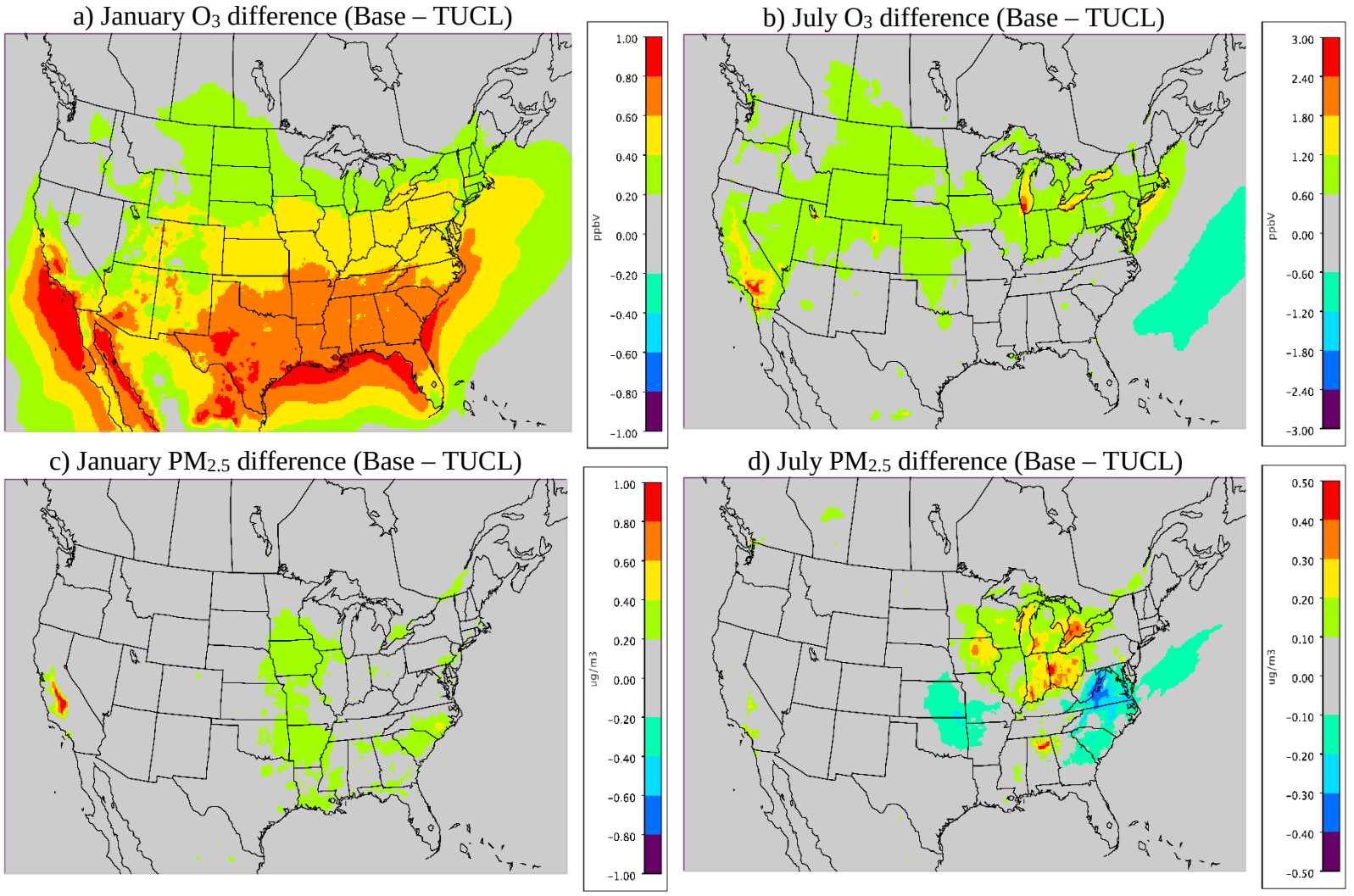

Figure 5: Difference in the monthly average O_3 for a) January and b) July and $PM_{2.5}$ (with organic matter mass removed) for c) January and d) July between CMAQ v5.1_Base and v5.1_TUCL (CMAQv5.1_Base – CMAQv5.1_TUCL). O_3 plots are in units of ppb and $PM_{2.5}$ plots are in units of μgm^{-3}. Note that the scales for each plot can vary.

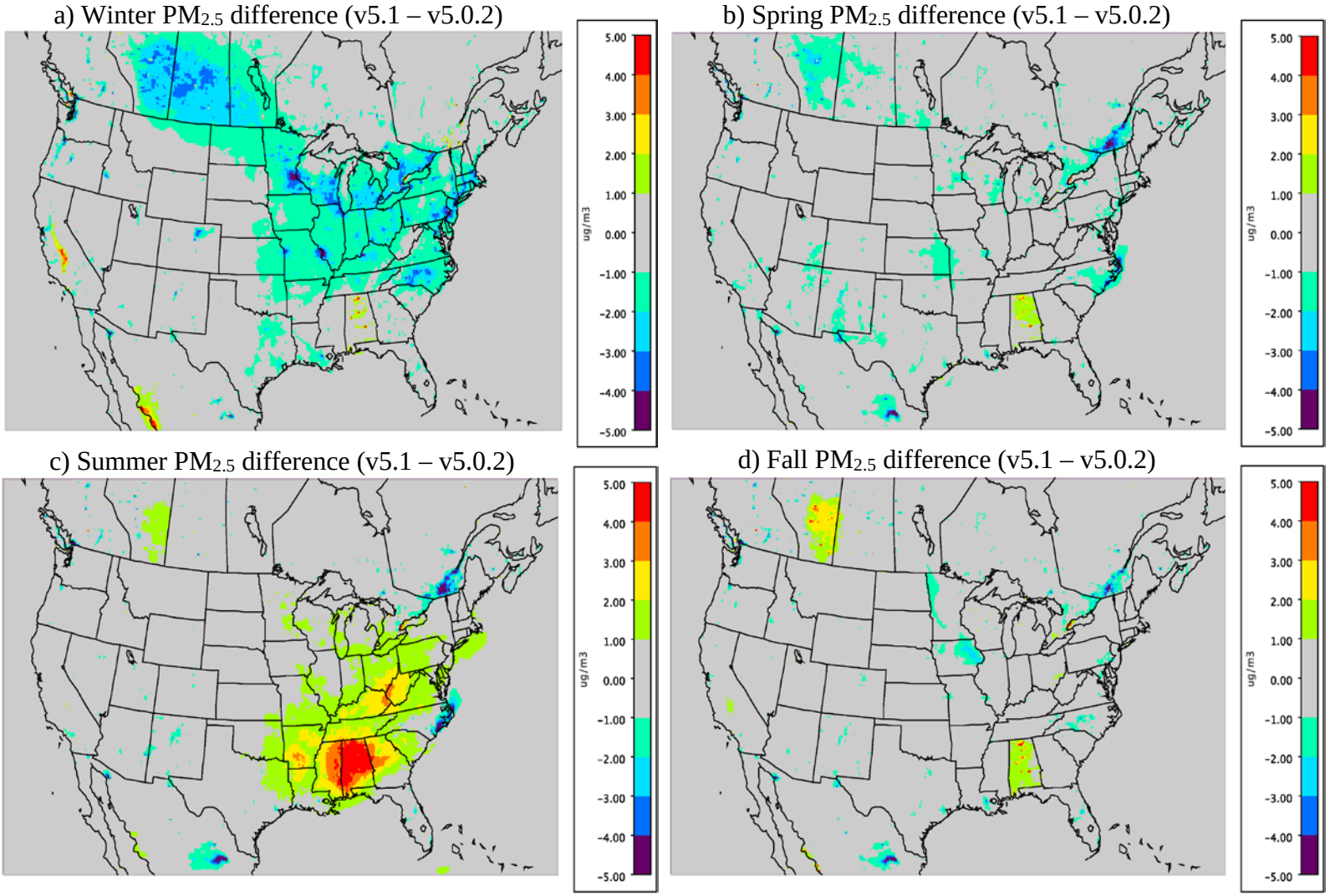

Figure 6: Difference in the seasonal average $PM_{2.5}$ for a) winter (DJF) b) spring (MAM) c) summer (JJA) and d) fall (SON) between CMAQ v5.0.2_Base and v5.1_Base (CMAQv5.1_Base – CMAQv5.0.2_Base). All plots are in units of μgm^{-3}.

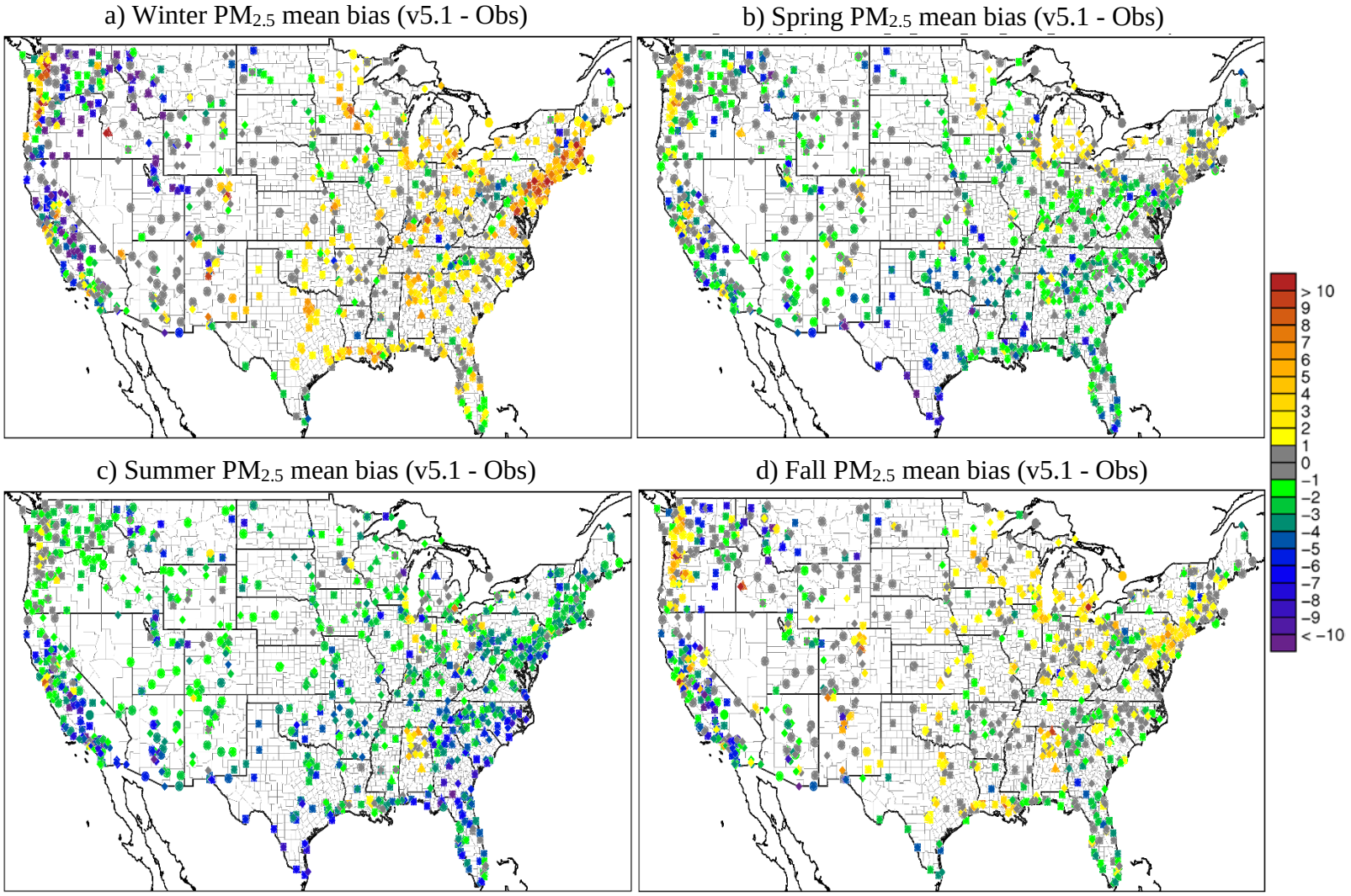

Figure 7: Seasonal average $PM_{2.5}$ mean bias (μgm^{-3}) at IMPROVE (circles), CSN (triangles), AQS Hourly (squares) and AQS Daily (diamonds) sites for a) winter (DJF) b) spring (MAM) c) summer (JJA) and d) fall (SON) for the CMAQ v5.1_Base simulation.

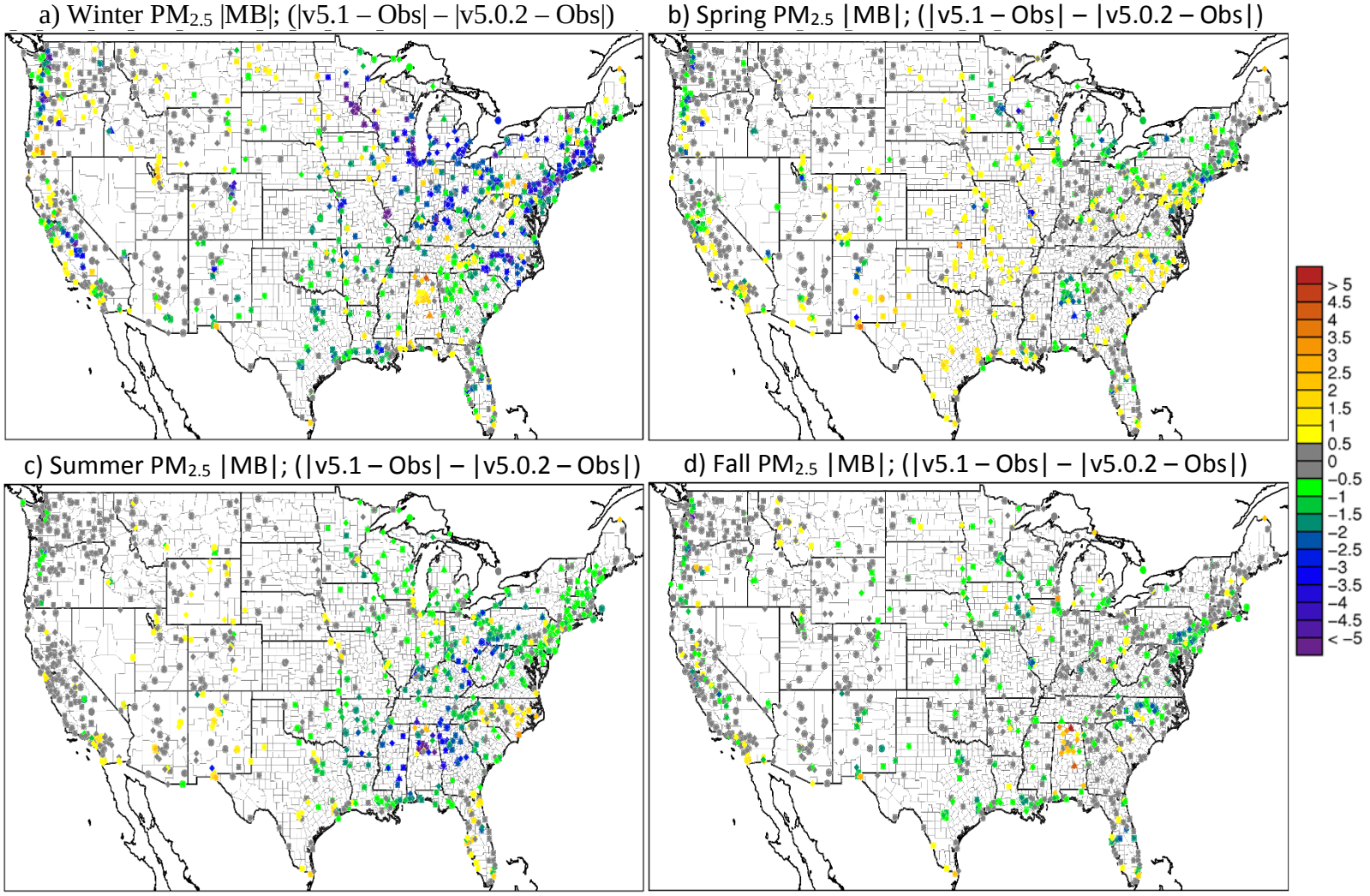

Figure 8: Difference in the absolute value of seasonal average $PM_{2.5}$ mean bias for a) winter (DJF) b) spring (MAM) c) summer (JJA) and d) fall (SON) between CMAQ v5.0.2_Base and v5.1_Base (CMAQv5.1_Base – CMAQv5.0.2_Base). All plots are in units of μgm^{-3}. Cool colors indicate a reduction in $PM_{2.5}$ mean bias in v5.1 while warm color indicate an increase in $PM_{2.5}$ mean bias v5.1.

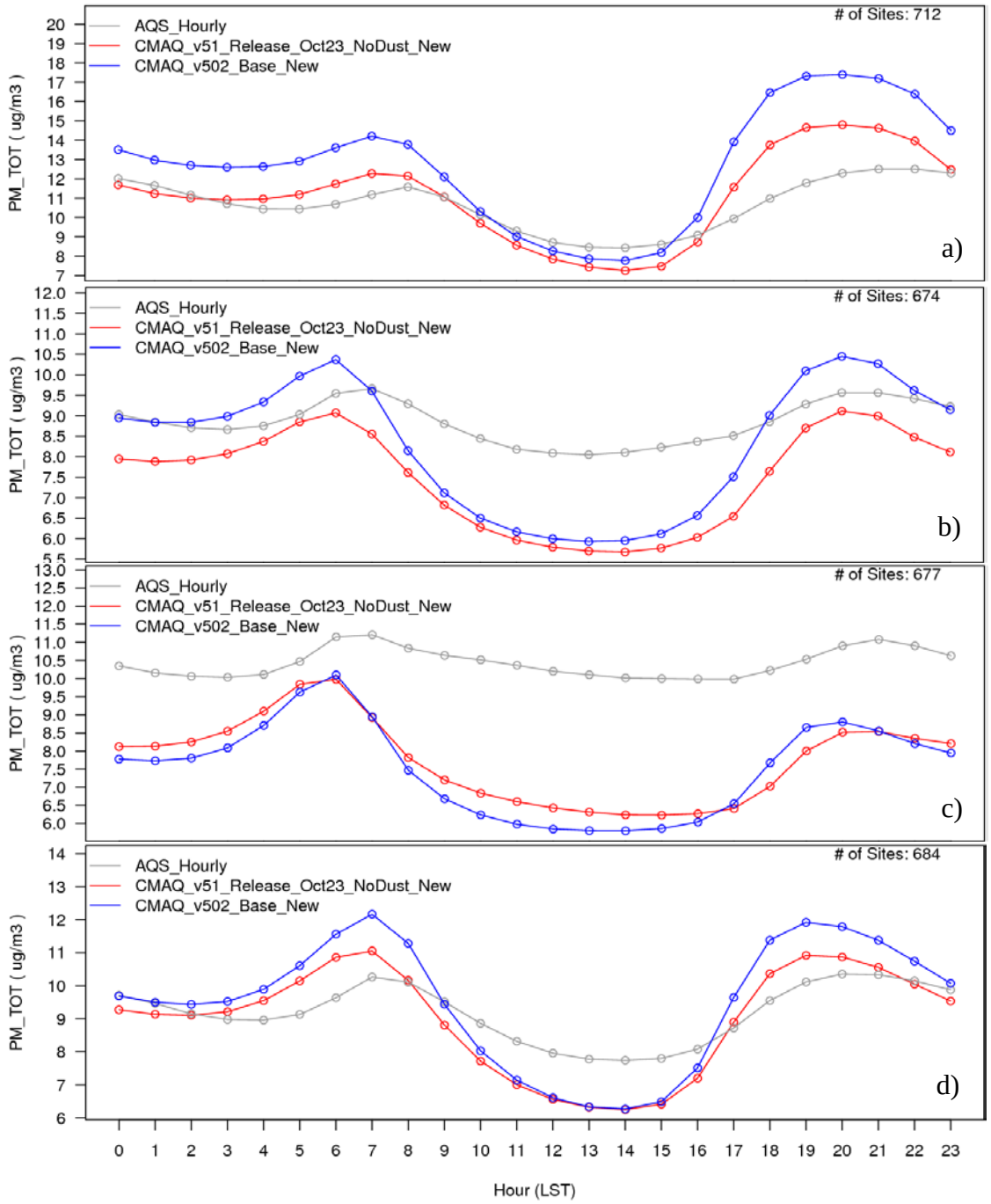

Figure 9: Diurnal time series of seasonal $PM_{2.5}$ (μgm^{-3}) from AQS observations (grey), CMAQv5.0.2_Base (blue) and CMAQv5.1_Base (red) for a) winter b) spring c) summer and d) fall.

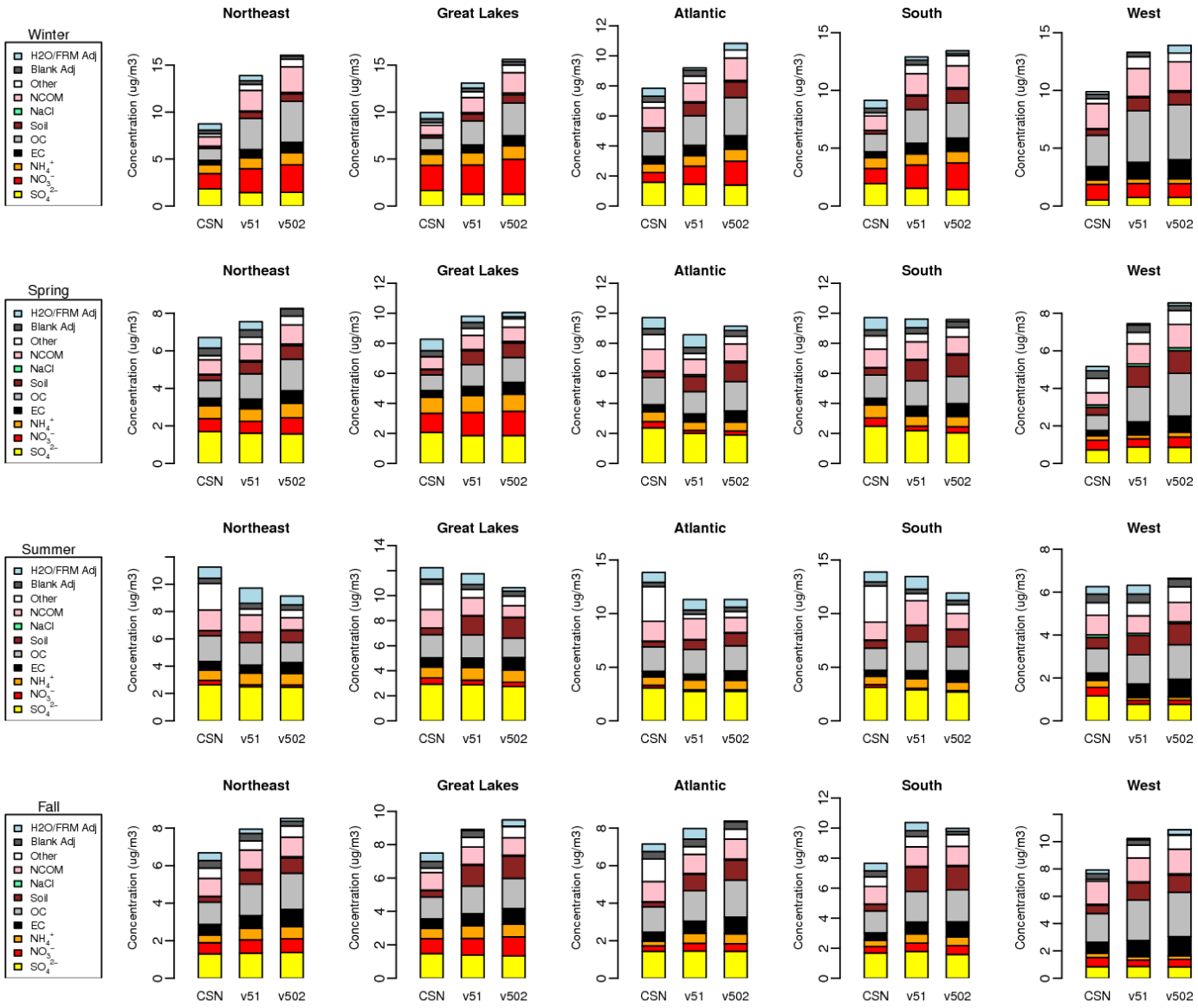

Figure 10: Regional and seasonal stacked bar plots of $PM_{2.5}$ composition at CSN sites. In order from top to bottom are spring, summer, fall and winter seasons and left to right the Northeast, Great Lakes, Atlantic, South and West regions. The individual $PM_{2.5}$ components (in order from bottom to top) are SO_4^{2-} (yellow), NO_3^- (red), NH_4^+ (orange), EC (black), OC (light gray), Soil (brown), NaCl (green), NCOM (pink), other (white), blank adjustment (dark gray) and H_2O/FRM adjustment (blue).

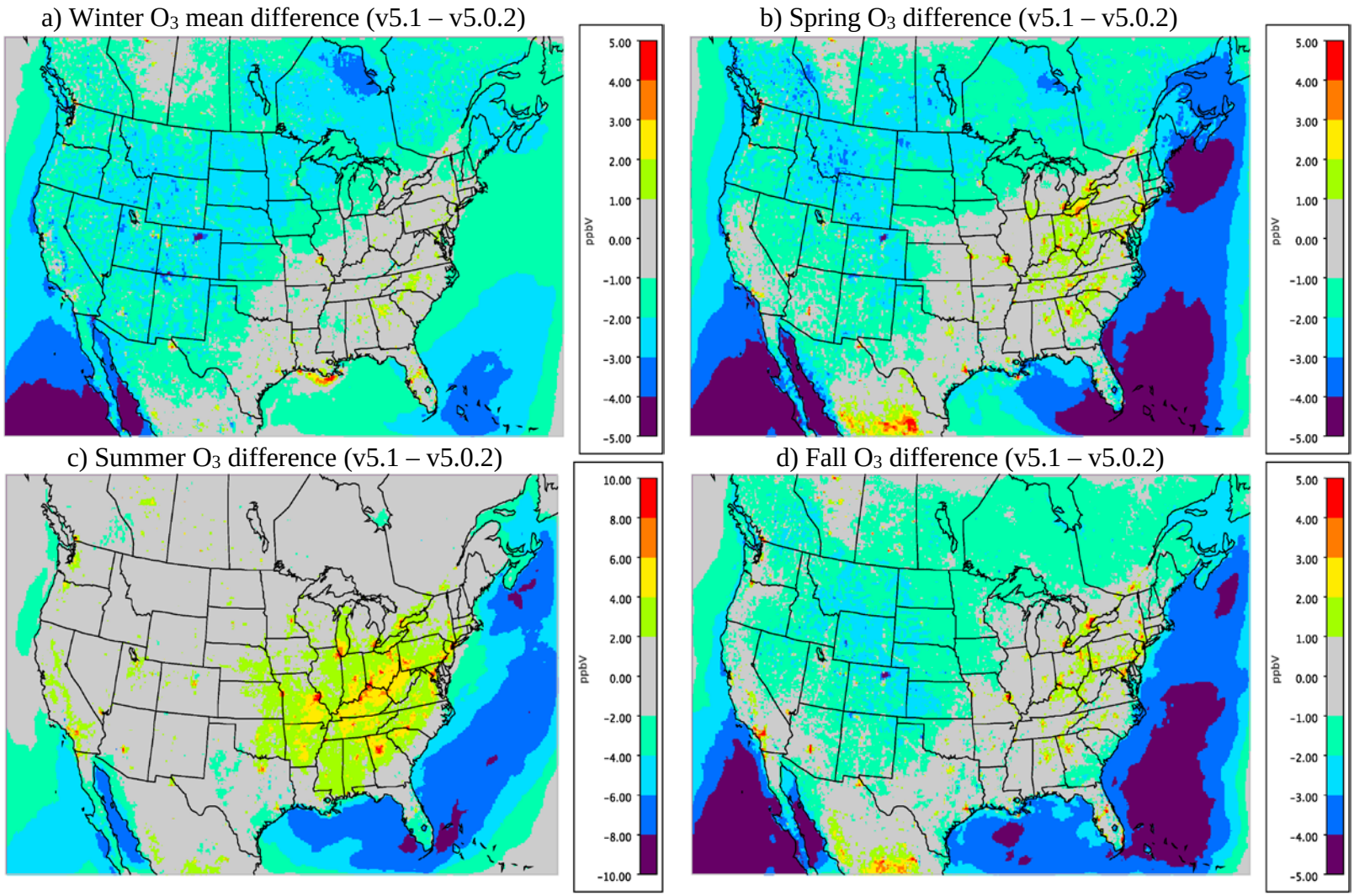

Figure 11: Difference in the monthly average hourly O_3 (ppbv) for winter (DJF; top left), spring (MAM; top right), summer (JJA; bottom left) and fall (SON; bottom right) between CMAQ v5.0.2_Base and v5.1_Base (CMAQv5.1_Base – CMAQv5.0.2_Base). Note that the scales for each plot can vary.

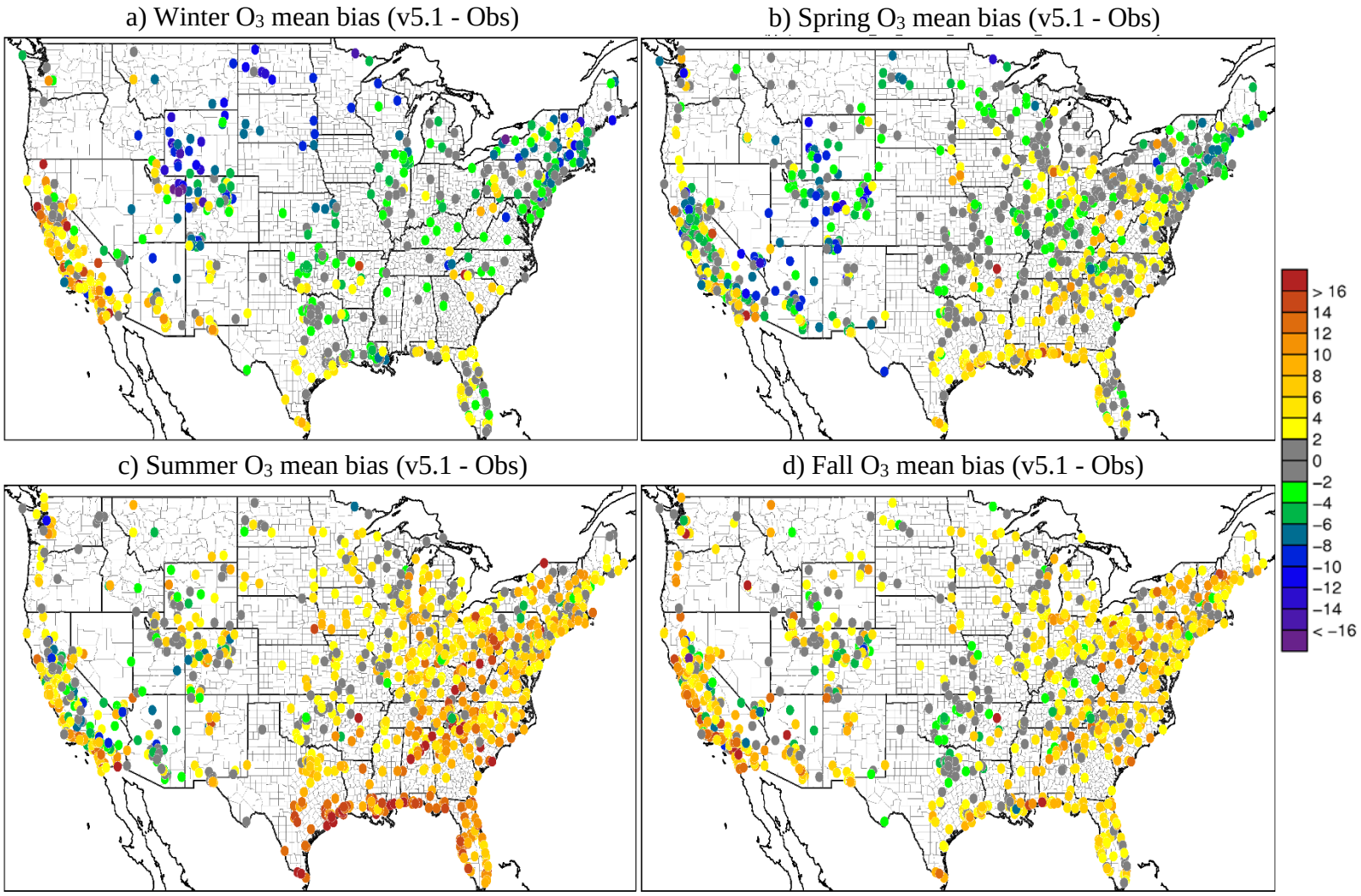

Figure 12: Seasonal average hourly O_3 mean bias at AQS sites for a) winter (DJF) b) spring (MAM) c) summer (JJA) and d) fall (SON) for the CMAQ v5.1_Base simulation. All plots are in units of ppbV.

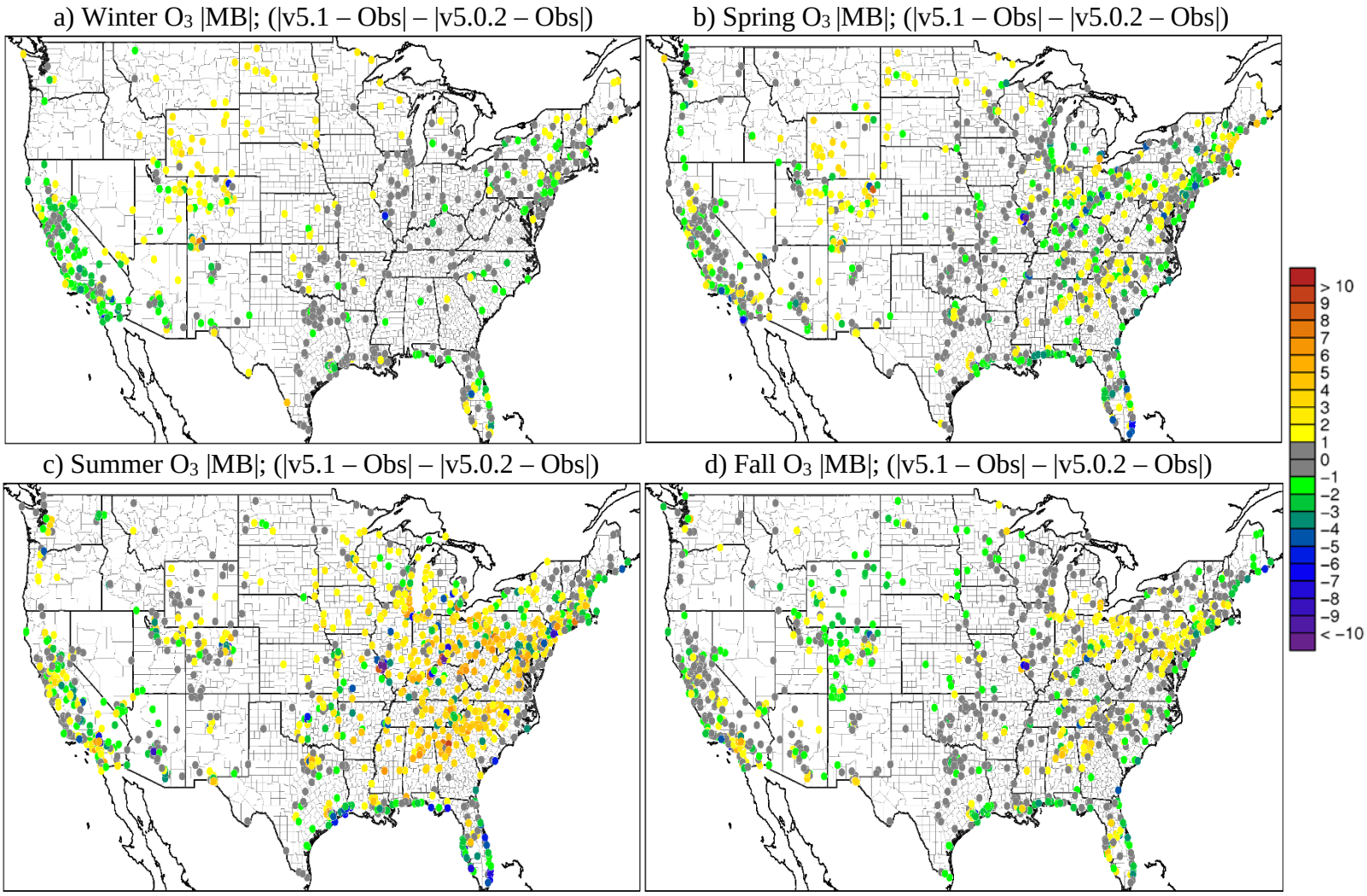

Figure 13: Difference in the absolute value of monthly average O_3 mean bias for a) winter (DJF) b) spring (MAM) c) summer (JJA) and d) fall (SON) between CMAQ v5.0.2_Base and v5.1_Base (CMAQv5.1_Base – CMAQv5.0.2_Base). All plots are in units of ppbV. Cool colors indicate a reduction in O_3 mean bias in v5.1 while warm color indicate an increase in O_3 mean bias v5.1.

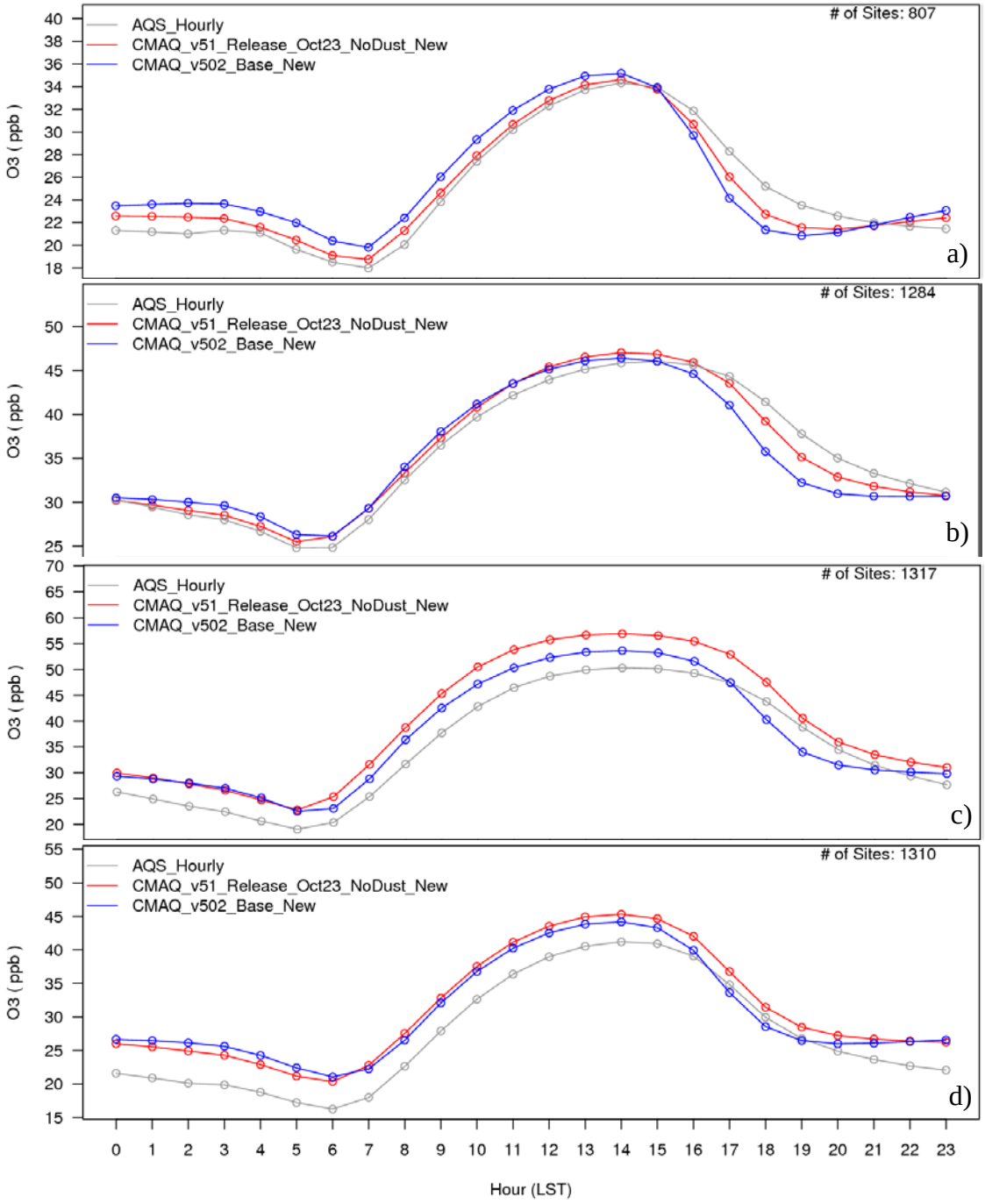

Figure 14: Diurnal time series of seasonal O_3 (ppbv) from AQS observations (grey), CMAQv5.0.2_Base (blue) and CMAQv5.1_Base (red) for a) winter b) spring c) summer and d) fall.

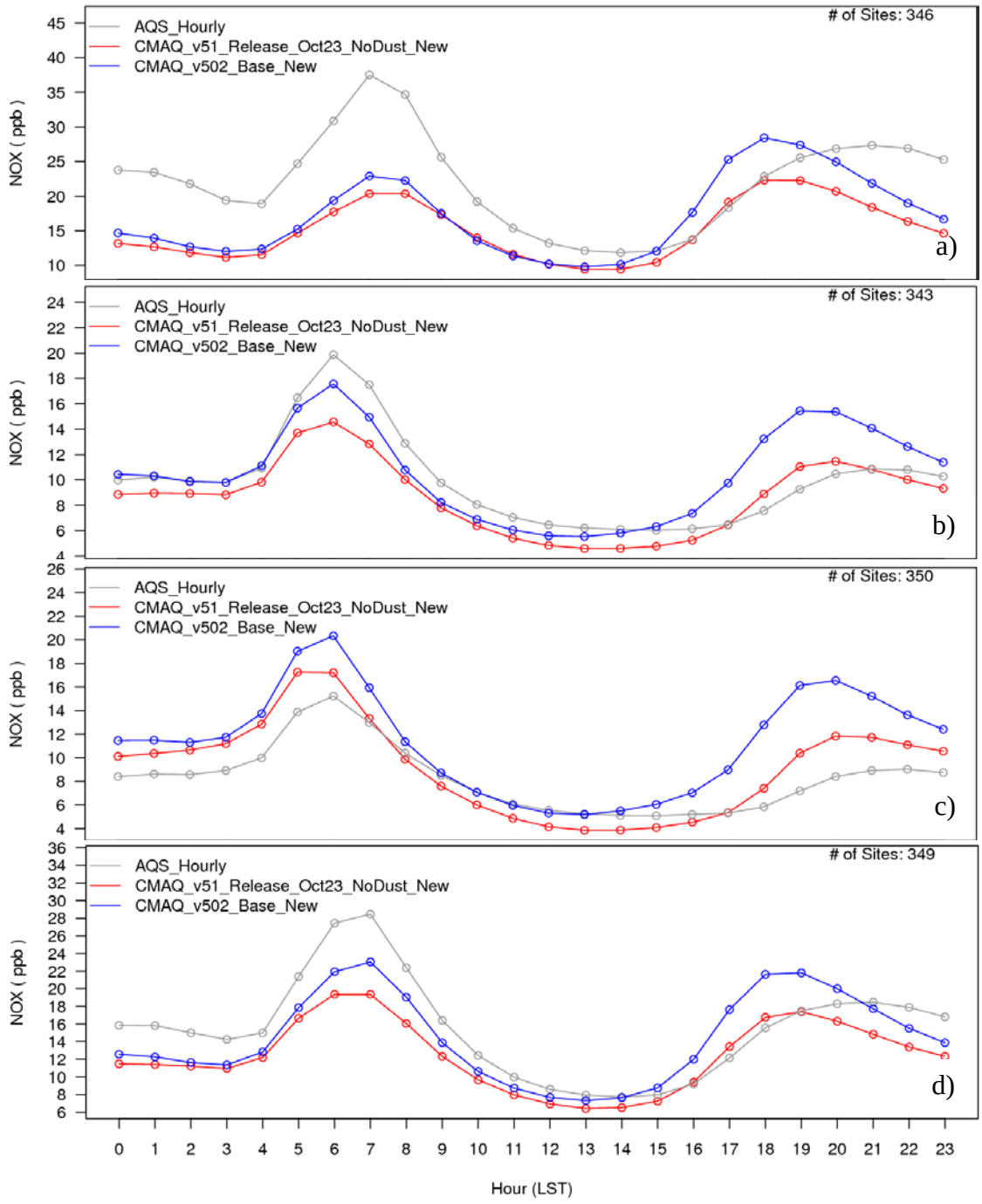

Figure 15: Diurnal time series of seasonal NO_X (ppbv) from AQS observations (grey), CMAQv5.0.2_Base (blue) and CMAQv5.1_Base (red) for a) winter b) spring c) summer and d) fall.

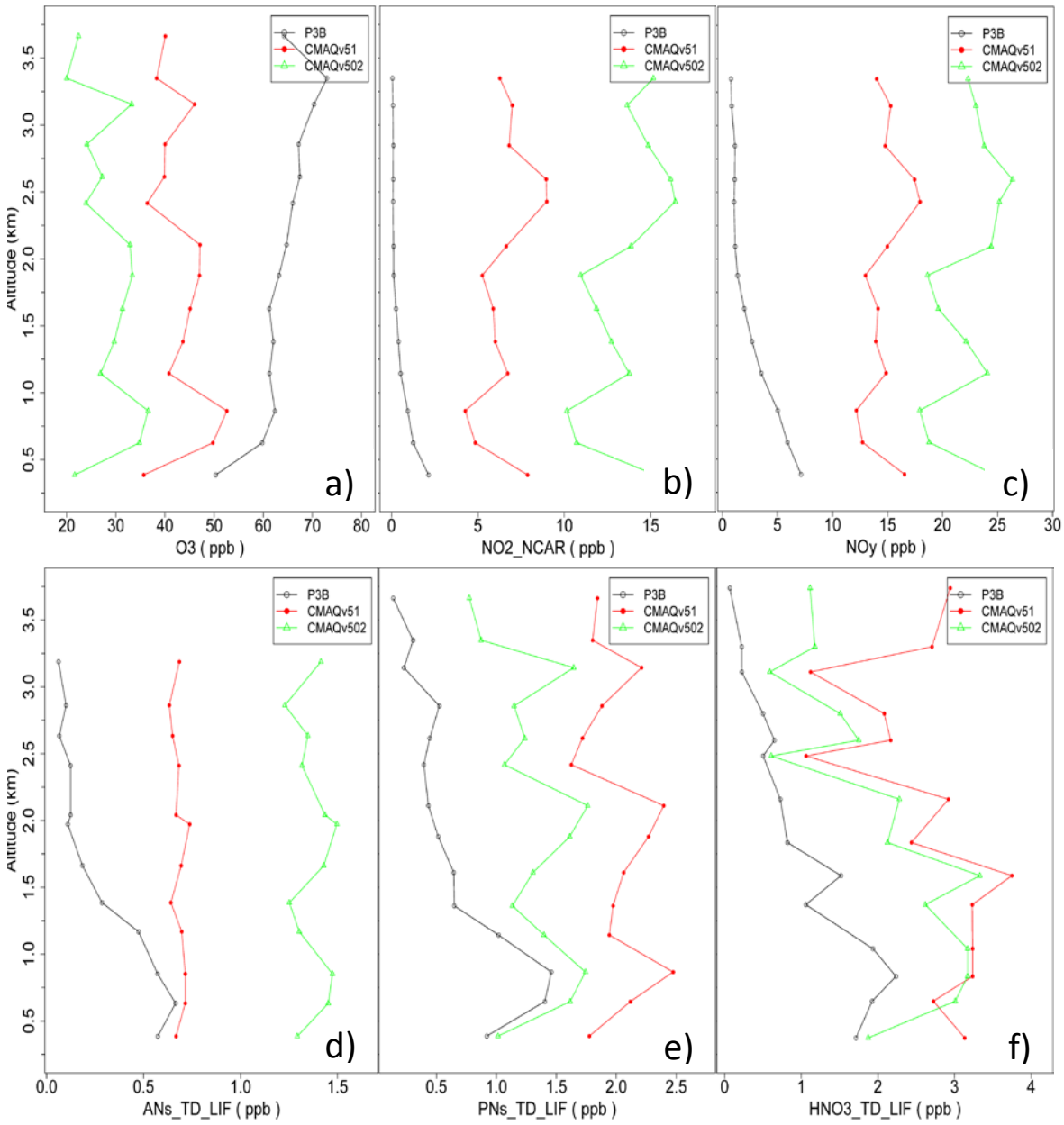

Figure 16: Observed (black) and CMAQ simulated vertical profiles of a) O_3 b) NO_2 c) NO_Y d) alkyl nitrates (ANs) e) peroxy nitrates (PNs) and f) HNO_3 for the Edgewood site in Baltimore, MD on July 5, 2011. CMAQv502_Base simulation profiles are shown in green and CMAQv51_Base simulation profiles are shown in red. Altitude (km) is given on the y-axis, while mixing ratio (ppbv) is given on the x-axis.

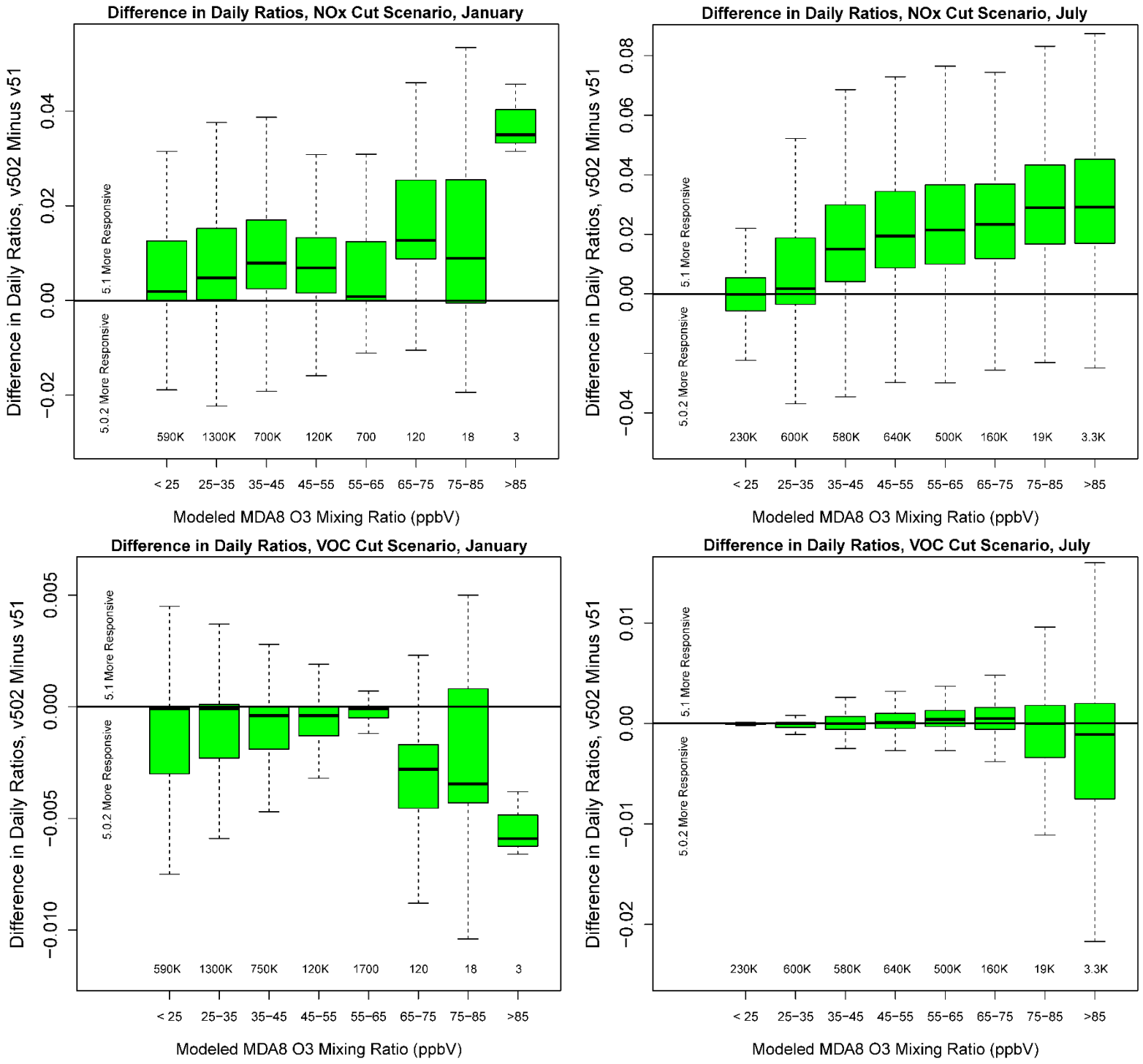

Figure 17: Difference in MDA8 O_3 daily ratios (Cut Scenario / Base) for CMAQv502 and v51 (v502 – v51) for a 50% cut in anthropogenic NO_x (top) and VOC (bottom) for January (left) and July (right) binned by the modeled MDA8 O_3 mixing ratio (ppbV). Values greater than one indicate v51 is more responsive than v502 to the emissions cut, while values less than one indicate v502 is more responsive. Given above the x-axis is the number of model grid cells in each bin.

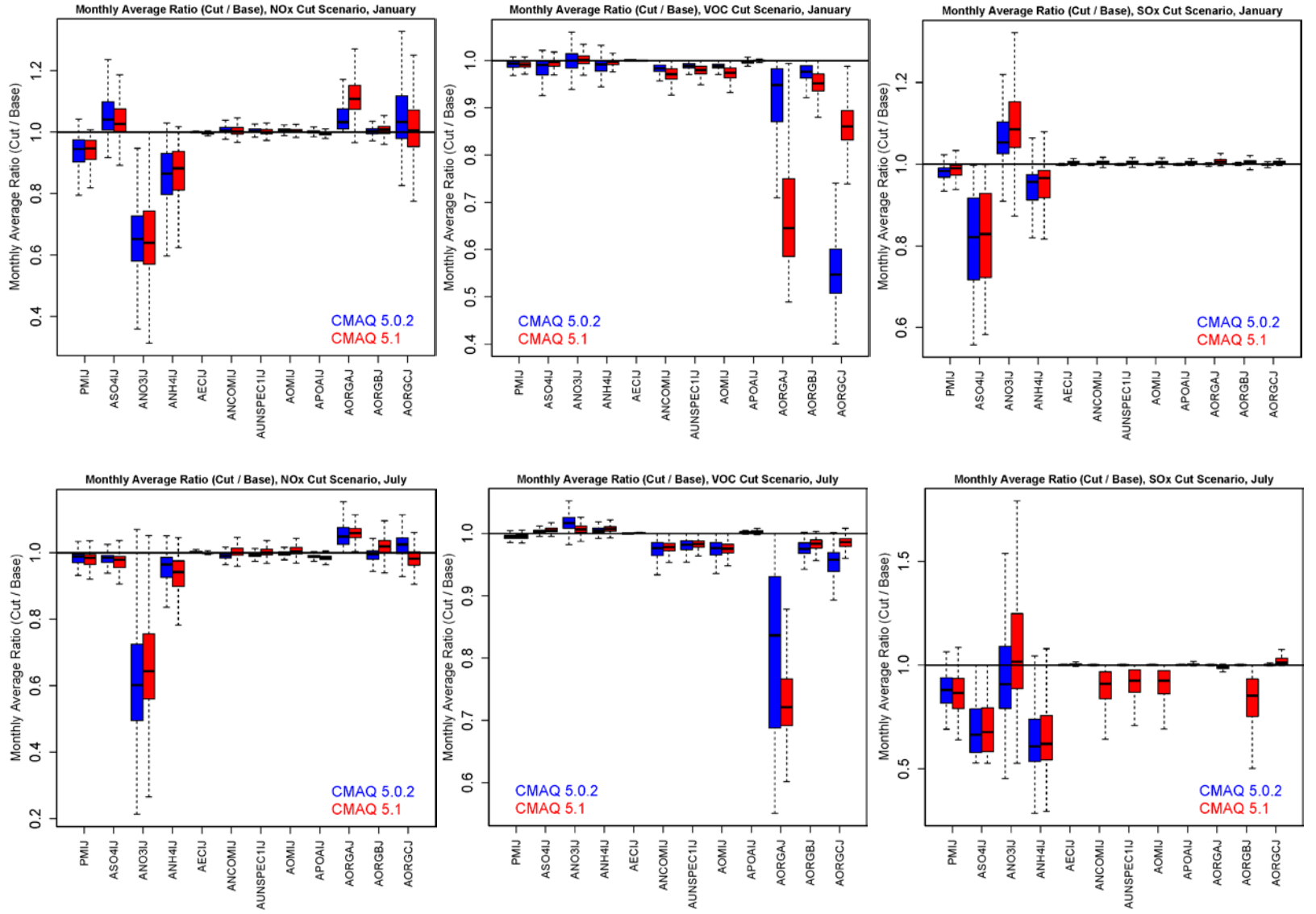

Figure 18: Box plots of monthly average ratio values (Cut /Base) of PMIJ (total $PM_{2.5}$), ASO4IJ, ANO3IJ, ANH4IJ, AECIJ, ANCOMIJ, AUNSPECIJ, AOMIJ, APOAIJ, AORGAJ, AORGBJ, and AORGCJ for v502 (blue) and v51 (red) for a 50% cut in anthropogenic NO_X (left), VOC (middle) and SO_X (right) for January (top) and July (bottom).